

Data assimilation by an intermediate coupled ocean-atmosphere model: Application to the 1997–1998 El Niño

Tong Lee

Jet Propulsion Laboratory, California Institute of Technology, Pasadena

Jean-Philippe Boulanger

Laboratoire d'Océanographie Dynamique et de Climatologie, CNRS, Université Paris VI, Paris

Alex Foo, Lee-Lueng Fu, and Ralf Giering

Jet Propulsion Laboratory, California Institute of Technology, Pasadena

Abstract. Sea surface temperature, sea level, and pseudo wind stress anomaly data from late 1996 to early 1998 are assimilated into an intermediate coupled model of the Tropical Pacific. Model data consistency is examined. Impact of the assimilation on forecast is evaluated. The ocean component of the coupled model consists of a shallow water model with two baroclinic modes, an Ekman shear layer, and a mixed layer temperature equation. The atmospheric model is a statistical one (based on dominant covariance of historical surface temperature and pseudo wind stress anomaly data). The adjoint method is used to fit the coupled model to 6 months of data by optimally adjusting the initial state and model parameters. A forecast is performed using the end state of an assimilation experiment as initial conditions and using parameters estimated during the assimilation period. Thus the model state during the assimilation and that during the forecast belong to the same model trajectory in different periods. Such an initialization procedure is useful in avoiding initial shock during forecast due to inconsistency of an initial state with the coupled model physics. As a result of optimal adjustments of initial state and parameters, the model is able to reproduce observed interannual variability of sea surface temperature and sea level reasonably well. The averaged residual model data misfits over various 6 month periods are 0.5°C and 5 cm, respectively. The model has a limited skill in reproducing much of the off-equatorial wind anomalies. The residual model data misfit in pseudo wind stress anomaly is larger than 10 m² s⁻². Forecasts initialized from the assimilation product are overall more realistic than those simply initialized from wind-forced ocean states. Consistent improvement due to optimal initialization is found for sea surface temperature and sea level anomalies in the central-eastern Pacific and zonal pseudo wind stress anomaly in the central Pacific, both in terms of root-mean-squared deviation from and correlation with the data. The adjustments of parameters in addition to initial state in a coupled context is found to be important to improving the model data consistency during the assimilation and the forecast. In particular, the estimated drag and damping coefficients properly regulate the relative strength of forcing and damping of the ocean state so as to fit the three types of observations during the assimilation (initialization) period, which facilitates the development of a large-amplitude warming event during the forecast. The study demonstrates the utility of oceanic and atmospheric data to estimate initial state and model parameters in a coupled context, which is useful to the evaluation, improvement, and initialization of El Niño–Southern Oscillation forecast models.

1. Introduction

Modern space-borne and in situ observing systems such as the altimeter onboard the TOPEX/Poseidon satellite and the Tropical Ocean–Global Atmosphere (TOGA)-Tropical Ocean–Atmosphere (TAO) array in the Tropical Pacific have provided an unprecedented capability to monitor El Niño–Southern Oscillation (ENSO) phenomenon, the most dominant climate variability of the ocean and atmosphere on sea-

sonal to interannual timescales. The data stream is also playing an important role in evaluating ENSO forecast models, improving their physics and parameterizations, and providing better initialization for forecasts.

A common approach to initializing a forecast model is to assimilate data into the stand-alone ocean component and to use the estimated ocean state to initialize the coupled ocean-atmosphere model. Examples include the system constructed by the National Centers for Environmental Prediction [Ji *et al.*, 1994a, 1994b; Ji and Leetmaa, 1997] on the basis of a coupled general circulation model and that constructed by Kleeman *et al.* [1995] on the basis of an intermediate coupled model. These studies have demonstrated the positive impact of ocean data

Copyright 2000 by the American Geophysical Union.

Paper number 2000JC900118.
0148-0227/00/2000JC900118\$09.00

assimilation on initializing ENSO forecasts. However, such an approach could lead to an initial state of the coupled model in which the oceanic state is not consistent with that of the atmosphere and hence limit the predictive skill by creating an “initial shock” in the forecast. This problem can be alleviated by assimilating data in a coupled mode in which the ocean and atmosphere states are adjusted simultaneously.

Such an attempt has been made by *Chen et al.* [1995] using the *Zebiak and Cane* [1987] model based on a fairly simple assimilation scheme in which the coupled model was nudged toward wind data to obtain initial states for forecasts. Significant improvement was found in the resultant prediction of the sea surface temperature anomaly in the central eastern Pacific. This improvement was attributed to the merit of initialization in a coupled mode that minimized initial shock. However, forecasts of the 1997–1998 El Niño using the same procedure showed little skill. *Chen et al.* [1998] argued that the cause for the poor forecast (of the 1997–1998 El Niño) was the lack of ocean data influence. An additional effort was reported first to assimilate sea level data (from tide gauge stations in the tropical Pacific Ocean) into the ocean component of the coupled model using a reduced space Kalman filter as described by *Cane et al.* [1996]. The coupled model was then nudged toward the resultant ocean states as well as wind data (as given by *Chen et al.* [1995]) to produce initial states for forecasts. The forecast of the sea surface temperature anomaly in the central eastern Pacific during the 1997–1998 El Niño period was improved as a result of this procedure. Apart from these two studies, applications of data assimilation in a coupled mode to initialization of ENSO prediction have not been reported. *Bennett et al.* [1998] employed a much more advanced method to assimilate optimally 1 year of thermocline depth, sea surface temperature, and wind data simultaneously into a modified *Zebiak and Cane* [1987] model. However, model-data consistency and reanalysis of the data were the objectives of that study, and no effort was made to evaluate the impact of the assimilation on forecasts.

The effort reported here is an initial attempt to assimilate several types of data simultaneously into a coupled model using an advanced assimilation scheme and to evaluate its impact on ENSO prediction. As a first step, the coupled model used here (as described later) is admittedly too simple, and the formulation of the assimilation can be further improved. The purpose of this effort is not to deliver a system for ENSO forecast. Instead, it is to explore an approach through which oceanic and atmospheric data are optimally assimilated by a coupled model, to evaluate the impact of the assimilation on forecast, and to understand how the impact was achieved. In contrast to previous studies that assimilated data into coupled models, model parameters and initial conditions are adjusted as part of the assimilation procedure.

Note that parameter estimation has been applied to simpler ocean (only) models but not to coupled atmosphere-ocean models. For instance, *Smestad and O'Brien* [1991] estimated the phase speeds of equatorial waves in a reduced gravity model; *Yu and O'Brien* [1991] estimated the wind stress drag coefficient and eddy viscosity profile using an Ekman layer model. Our results highlight the importance of parameter estimation in a coupled mode to improving model fits to data as well as to improving prediction. Moreover, they serve to evaluate the impact of such data assimilation on ENSO forecast and to isolate factors that limit the skills of the model because

of the lack of data influence from those due to incomplete model physics.

The paper is organized as follows. Various components of the coupled model, the data to be assimilated, and the assimilation method are described in sections 2, 3, and 4, respectively. Results of the assimilation experiments are discussed in section 5. Hindcasts/forecasts initialized from the assimilation products are presented in section 6. The role of parameter estimation in fitting model to data, in forecasting, and in modifying the coupling regimes is further addressed in section 7. The findings are summarized in section 8.

2. Model

Our coupled model is an “anomaly” type: it is meant to describe the evolution of interannual anomaly relative to a prescribed “background” seasonal cycle. Examples of an anomaly model include those used by *Zebiak and Cane* [1987], *Battisti* [1988], and *Kleeman et al.* [1995]. This subsection describes the components of our (anomaly) coupled model and the determination of the climatological seasonal cycle.

The ocean basin covers the tropical Pacific, extending from 128° to 278°E in longitude and from 28.75°S to 28.75°N in latitude. The resolution is 2° in longitude and 0.5° in latitude. The model has a rectangular basin and therefore does not include any coastline. The ocean model has three components: (1) a linearized shallow water equation on an equatorial beta plane solved in terms of two baroclinic modes to reflect the low-frequency motions associated with wind-forced Kelvin and Rossby waves, (2) an Ekman shear layer to include the surface enhancement of frictional current by direct wind forcing, and (3) a simplified mixed layer thermodynamic equation that uses the sum of the baroclinic and Ekman currents in the mixed layer to simulate the evolution of the mixed layer temperature, taken as sea surface temperature (SST). All components use a leapfrog time-stepping scheme with a 5 day time step, in contrast to the *Zebiak and Cane* [1987] model, which uses a forward scheme and a 10 day time step. The atmospheric component is a statistical model. Such a coupled model is simpler than the usual “intermediate” type [e.g., *Zebiak and Cane*, 1987; *Kleeman*, 1993] in the atmospheric component, simpler than the “hybrid” type [*Neelin*, 1990; *Barnett et al.*, 1993] in the oceanic component, and much simpler than coupled general circulation models [*Ji et al.*, 1994b; *Kirtman et al.*, 1997]. The reasons for choosing such a coupled model for the initial effort are (1) it serves as a baseline to evaluate the performance of more complete models, (2) it allows an investigation of the limits of simple physics in accounting for various observations and in delivering prediction when prior observational data have been assimilated, and (3) its relatively clear coding structure facilitates the construction of an advanced assimilation scheme.

In the coupled model the variables computed by all components are interannual anomalies. The seasonal climatology of a variable, where needed, is prescribed. However, the baroclinic and shear layer components can be run off-line and forced by a prescribed total wind product to generate total current. This is, in fact, how we obtained the climatological seasonal current, which is then prescribed to the coupled (anomaly) model (as discussed in section 2.5).

2.1. Baroclinic Component

Let u_b , v_b , and h_b denote the baroclinic components of the zonal current, meridional current, and sea level, and τ^x and τ^y

denote the zonal and meridional surface wind stress, the baroclinic model equations can be written as

$$\frac{\partial u_b}{\partial t} - \beta y v_b + g \frac{\partial h_b}{\partial x} = \frac{\tau^x}{\rho_0 H_{eq}} - r_b u_b, \quad (1)$$

$$\beta y u_b + g \frac{\partial h_b}{\partial y} = \frac{\tau^y}{\rho_0 H_{eq}} - r_b v_b, \quad (2)$$

$$\frac{\partial h_b}{\partial t} + c^2 \left(\frac{\partial u_b}{\partial x} + \frac{\partial v_b}{\partial y} \right) = -r_b h_b, \quad (3)$$

where H_{eq} , c , and r_b are the equivalent depth, wave speed, and Rayleigh friction constant, respectively, of a baroclinic mode. H_{eq} and c are related by $c^2 = gH_{eq}$ (where g is the gravitational acceleration). The equations are the same for both modes except for differences in c (and thus H_{eq}) and r_b : c being 2.8 and 1.3 m s⁻¹ and r_b being the reciprocal of 12 and 6 months for modes 1 and 2, respectively. The phase speed for the first mode is very close to that used in the *Zebiak and Cane* [1987] model. The frictional timescales are chosen following *Picaut et al.* [1993]. Note that these timescales are much shorter than that used in the *Zebiak and Cane* [1987] model (30 months). *Perigaud and Dewitte* [1996] also reported that for the *Zebiak and Cane* [1987] model in a forced mode, a 9 month frictional timescale results in better comparison of sea level anomaly with observations than the original 30 month one does. The sum of the solutions for the two modes gives rise to the total baroclinic horizontal velocity and sea surface height anomalies (SSHA). The baroclinic equations are solved in a way similar to that described by *Cane and Patton* [1984]. The solution is split into a Kelvin part and a non-Kelvin part (long Rossby waves and anti-Kelvin waves propagating along the southern and northern boundaries of the ocean model). The Kelvin part is integrated from the western boundary to the eastern boundary; the non-Kelvin part integrated from the eastern boundary to the western boundary. Such a scheme allows the use of a large time step (presently 5 days).

2.2. Shear Layer Module

Following *Blumenthal and Cane* [1989], a shear layer model is used to compute the wind-forced surface current contribution not estimated by the baroclinic model. Introducing (u_s, v_s) as the shear currents, the shear layer model equations are

$$\frac{\partial u_s}{\partial t} - \beta y v_s = \frac{\tau^x}{\rho_0} \left(\frac{1}{H_{ML}} - \frac{1}{H} \right) - r_s u_s, \quad (4)$$

$$\frac{\partial v_s}{\partial t} + \beta y u_s = \frac{\tau^y}{\rho_0} \left(\frac{1}{H_{ML}} - \frac{1}{H} \right) - r_s v_s, \quad (5)$$

where H_{ML} is the mixed layer depth (50 m), H is $(H_1^{-1} + H_2^{-1})^{-1}$ (H_1 and H_2 are both 200 m), and r_s is a Rayleigh friction taken to be the reciprocal of 2 days (same as that used in the *Zebiak and Cane* [1987] model). The shear layer solution is computed on the same grid as the baroclinic model. The shear current and baroclinic current sum up to the total horizontal surface current in the mixed layer, $u + v$. Vertical velocity w at the base of the mixed layer is diagnosed from u and v using the continuity equation. These horizontal and vertical velocities will be used in the computation of SST evolution to be described next.

2.3. Mixed Layer SST Component

The surface temperature anomaly in the mixed layer is computed on a C grid, with a spatial resolution identical to the baroclinic component previously described, over the domain of 129°–277°E and 28.5°S to 28.5°N. The equation is similar to that of the *Zebiak and Cane* [1987] ocean model but has different subsurface temperature parameterization:

$$\begin{aligned} \frac{\partial T}{\partial t} = & - \frac{\partial[(\bar{u} + u)T]}{\partial x} + T \frac{\partial(\bar{u} + u)}{\partial x} - \frac{\partial(u\bar{T})}{\partial x} + \bar{T} \frac{\partial u}{\partial x} \\ & - \frac{\partial[(\bar{v} + v)T]}{\partial x} + T \frac{\partial(\bar{v} + v)}{\partial x} - \frac{\partial(v\bar{T})}{\partial x} + \bar{T} \frac{\partial v}{\partial x} \\ & + \frac{[M(\bar{w} + w) - M(\bar{w})](\bar{T} - \bar{T}_{sub})}{H_{ML}} \\ & - \frac{M(\bar{w})(T - T_{sub})}{H_{ML}} - r_T T. \end{aligned} \quad (6)$$

Quantities with and without the overbar correspond to the seasonal climatology and interannual anomalies, respectively. The first four terms in (6) are mathematically equivalent to $(\bar{u} + u) \partial T / \partial x + u \partial T / \partial x$ (advection of temperature anomaly by total zonal current plus advection of climatological temperature by anomalous zonal current). However, this form is numerically not as accurate as the four-term form in (6). $M(x)$ is a mixing function such that $M(x) = x$ if $x > 0$ and $M(x) = 0$ if $x < 0$, r_T is a Rayleigh friction taken to be the reciprocal of 125 days (same as that used in the *Zebiak and Cane* [1987] model). T_{sub} is the subsurface temperature at the base of the mixed layer being advected into the mixed layer. The subsurface temperatures \bar{T}_{sub} and T_{sub} are parameterized as follows. First, the actual mixed layer depth H_{ML}^{obs} , defined as the depth at which the subsurface temperature is 0.5°C less than the surface temperature [cf. *Levitus*, 1982], is first determined at every grid point and every month from expandable bathythermograph (XBT) data for the period of 1980–1994 [*Smith*, 1995]. A subsurface temperature is then derived by requiring the vertical temperature gradient across the 50 m model mixed layer depth to be equal to that across the actual mixed layer: $SST - 0.5 H_{ML} / H_{ML}^{obs}$. Such a subsurface temperature field is then separated into the seasonal climatology \bar{T}_{sub}^{obs} and the interannual anomaly T_{sub}^{obs} . The former is prescribed as \bar{T}_{sub} in (6). The latter is used to compute the interannual anomaly of dynamic height h^{obs} . The model's subsurface temperature anomaly T_{sub} is parameterized in terms of the model's height anomaly h through the following analytical relation

$$T_{sub} = a_+ \tanh(b_+ h), \quad h > 0,$$

$$T_{sub} = a_- \tanh(b_- h), \quad h < 0,$$

where the four coefficients a_+ , a_- , b_+ , and b_- are estimated at each grid point by optimizing the fit of T_{sub}^{obs} to h^{obs} . A more complete description of the subsurface temperature parameterization is given by *Boulanger* [2000].

2.4. Atmospheric Component and Coupling

The statistical atmosphere model is similar to the one described by *Syu et al.* [1995]. The spatial covariance between observed sea surface temperature anomaly (SSTA) compiled by the National Oceanic and Atmospheric Administration (NOAA) Climate Analysis Center and the pseudo wind stress

anomaly (PWSA) data compiled by the Florida State University (FSU) are calculated for the region within $\pm 15^\circ$ of the equator over the period 1980–1995. Singular value decomposition (SVD) is applied to computing the dominant modes of the covariability. *Syu et al.* [1995] found that the first seven modes account for 80–90% of the total interannual variance, with the variance of the first mode 4 times larger than that of the second mode. Their choice to use the first seven modes is somewhat arbitrary. In our study, only the first four modes are used as we found little difference in the overall behaviors of 1 year forecasts using the first four and the first seven modes. Let $T_n(x, y)$ and $\hat{\tau}_n(x, y)$ denote the spatial singular vectors for SSTA and PWSA (both for the zonal and meridional components) for the n th mode, respectively, and let $a_T(t)$ and $a_{\hat{\tau}}(t)$ denote the (best fitted) amplitude time series of the corresponding mode. The observed SSTA and PWSA can be approximated by

$$T_d(x, y, t) \approx \sum_{n=1}^4 T_n(x, y) a_n^T(t) \quad (7)$$

$$\hat{\tau}_d(x, y, t) \approx \sum_{n=1}^4 \hat{\tau}_n(x, y) a_n^{\hat{\tau}}(t). \quad (8)$$

Let $\sigma_{\hat{\tau}}^n$ and σ_T^n represent the rms amplitude of $\hat{\tau}_n(x, y)$ and $T_n(x, y)$, respectively; $\alpha^n = \sigma_{\hat{\tau}}^n / \sigma_T^n$, the model's wind stress anomaly, is generated as follows.

First, the model SSTA, $T_m(x, y, t)$, is projected onto the SSTA singular vectors by

$$A_n(t) = \int^{xy} T_m(x, y, t) T_n(x, y) dx dy. \quad (9)$$

The model's PWSA is then determined through

$$\hat{\tau}_m(x, y, t) = \sum_{n=1}^N A_n(t) \alpha_n \hat{\tau}_n(x, y). \quad (10)$$

Note that model PWSA is generated only for the region within $\pm 15^\circ$ of the equator because the SVDs are only computed for this area. The wind outside $\pm 15^\circ$ is determined by tapering off the values at $\pm 15^\circ$ (at each longitude) away from the equator with a Gaussian function. Therefore the region outside $\pm 15^\circ$ of the equator is more of a buffer zone. The PWSA is converted to the wind stress anomaly that drives the ocean model through the bulk formula $\rho_a c_d \hat{\tau}_m$, where ρ_a is air density (1.2 Kg m^{-3}) and c_d is the drag coefficient. The value of c_d is chosen to be 1.2×10^{-3} , the same as that used by *Syu et al.* [1995].

To facilitate subsequent discussion about the role of the various SVD modes, the spatial SVDs of the four modes are shown in Plate 1. Mode 1 (Plates 1a (left) and 1a (right)) describes the covariability between zonal wind stress variability in the central Pacific and that of SST in the central-eastern Pacific. Mode 2 (Plates 1b (left) and 1b (right)) reflects the covariability between zonal wind stress in the central-eastern Pacific and that of SST near the eastern boundary (off South America). These two modes highlights the “central-eastern” and “eastern” warming, respectively, which are known to differ in magnitude and timing among different El Niño events. The patterns of modes 3 and 4 are more difficult to interpret (although mode 3 appears to be somewhat similar to mode 2).

Note that an SVD mode alone, especially toward higher mode, does not necessarily represent any physics because they are simply statistical basis functions that are orthogonal to one another.

2.5. Seasonal Climatology

There are five seasonal climatologies needed (all of them used in (6)) in order to run the coupled model: \bar{T} , \bar{T}_{sub} , \bar{u} , \bar{v} , and \bar{w} . \bar{T} is determined from monthly SST data from 1980 to 1996 compiled by the NOAA Climate Analysis Center. The determination of \bar{T}_{sub} was discussed in section 2.3. The specification of \bar{u} , \bar{v} , and \bar{w} , ideally, should also be based on observations. Unfortunately, there is no observation of the vertical velocity. In the present study the climatological current is obtained from an extended run of the baroclinic and the shear layer model forced by the seasonal climatology of the full wind stress compiled by FSU. In Figure 1, the model's climatological surface current in April and October are compared with *Reverdin et al.*'s [1994] analysis of climatological seasonal current at 15 m depth based on drifting buoy and current meter data (available through the International Research Institute (IRI)/Lamont-Doherty Earth Observatory (LDEO) Climate Data Library site <http://ingrid.ldeo.columbia.edu>). Note that the data have a much coarser resolution than the model. The model's South Equatorial Current (SEC), North Equatorial Countercurrent (NECC), and the North Equatorial Current (NEC) in both seasons bear much resemblance to the observed climatology. For example, both the model and data show a “split” of the westward SEC into a northern and a southern branch by an equatorial eastward flow east of 200°E in April but not in October. The model's currents are generally weaker than the observational counterparts, probably because of the lack of nonlinearity or frictional timescales being too short in the ocean model.

2.6. Initialization

The initial state of the coupled model consists of initial SSTA, components of SSHA, and anomalous current associated with the Rossby and Kelvin solutions for different modes. The atmospheric state (wind stress) is not part of the initial state. Conventionally, an initial state is obtained by forcing the ocean model with observed wind. A somewhat different strategy is used here. The ocean model is forced by a “statistical” wind anomaly generated from the projection of observed SSTA onto the SVDs. This is different from a coupled run because PWSA is generated by observed (as opposed to model) SSTA through the SVDs. Comparing to forcing the ocean model by observed wind stress anomaly, this initialization approach is more consistent with the coupled model and is less likely to produce initial shock in a forecast. The resultant ocean states are used as prior initial conditions for the assimilation experiments to be described in section 4. Throughout the text, the units of SSHA, SSTA, and PWSA are all centimeter, degree, and $\text{m}^2 \text{ s}^{-2}$, respectively.

3. Data

Three types of data are assimilated into the coupled model: SSH, SST, and wind stress. All data used are monthly averages and are mapped to the model grid described in section 2. The SSH data used are from the TOPEX/Poseidon altimeter [*Fu et al.*, 1994]. SST data, obtained from a Columbia University Web site <http://ingrid.ldeo.columbia.edu/SOURCES>, were com-

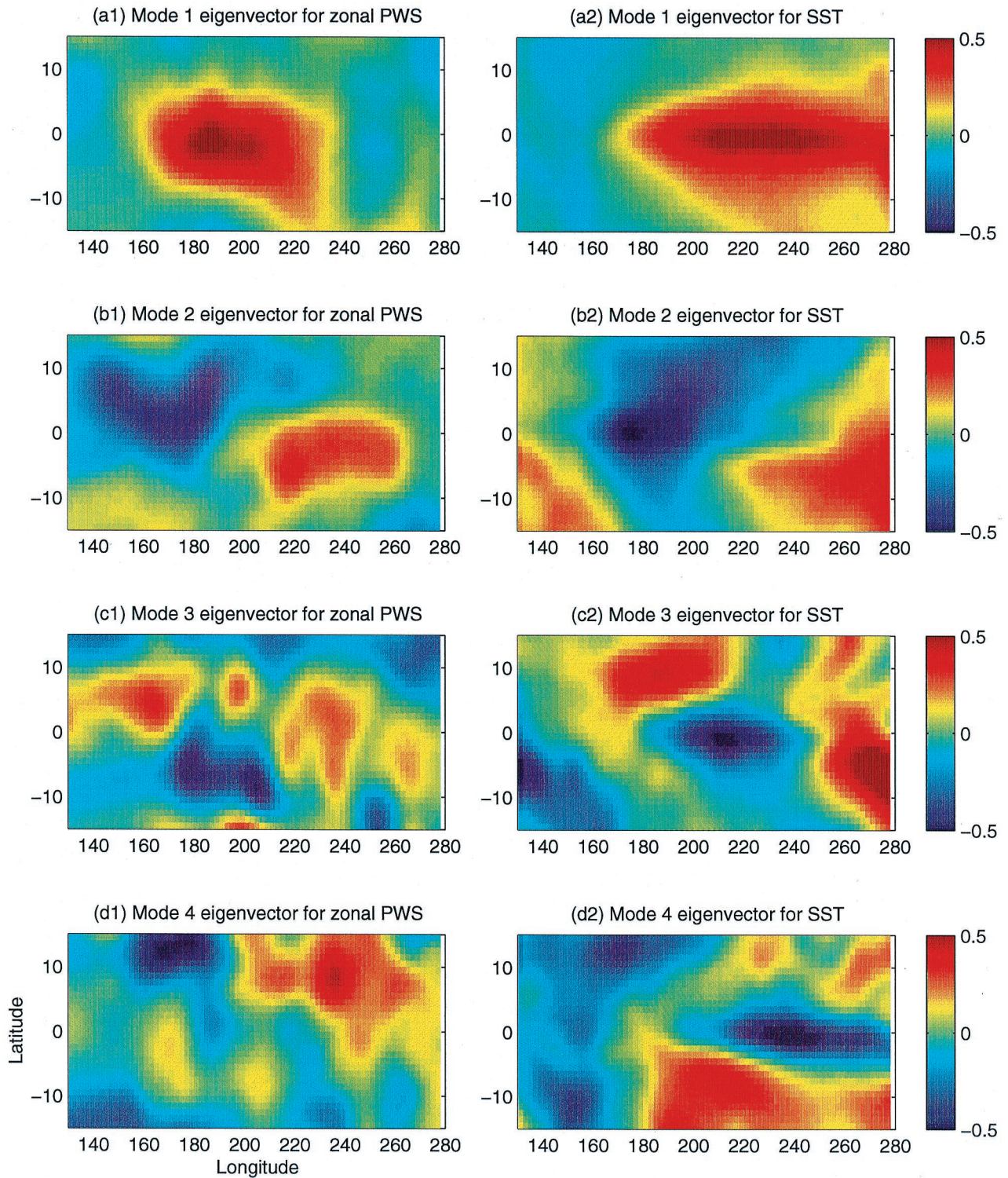


Plate 1. The four modes of SVD for (left) zonal pseudo wind stress and (right) SST. Modes 1 and 2 reflect warming in the central-eastern and eastern Pacific, respectively.

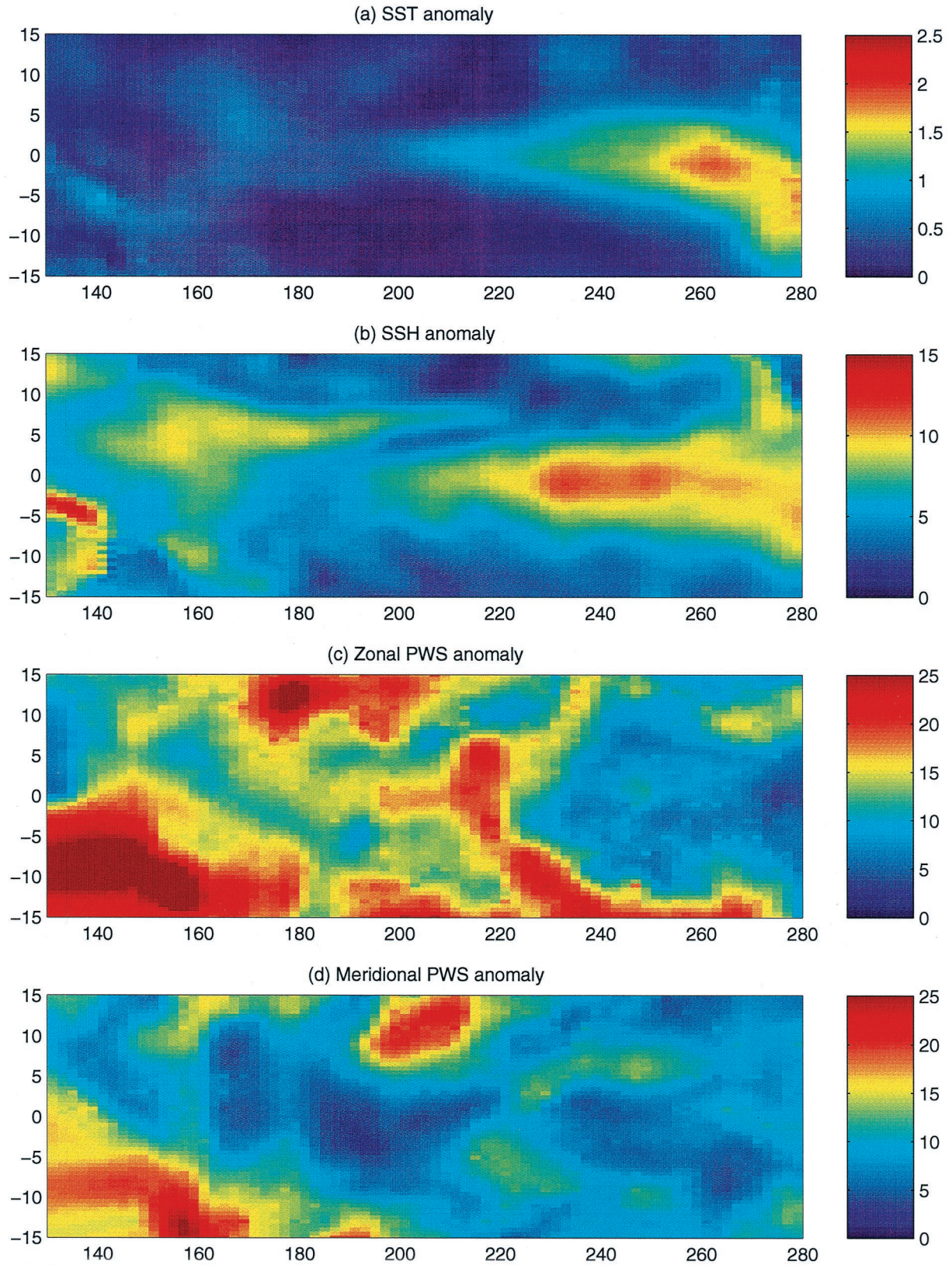


Plate 2. Rms differences between simulation and data for (a) surface temperature, (b) sea level, (c) zonal, and (d) meridional pseudo wind stress anomalies.

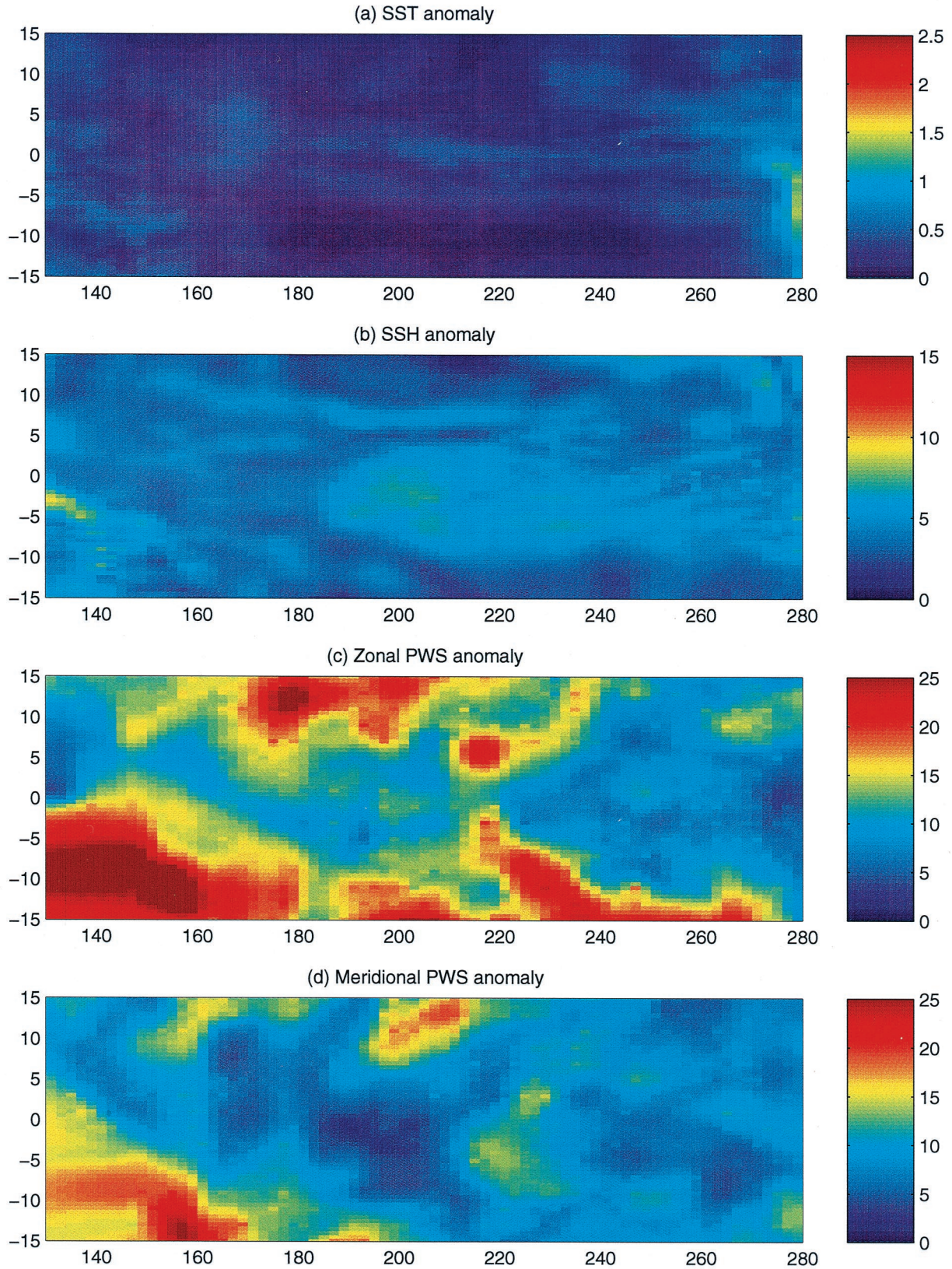


Plate 3. Rms differences between assimilation and data for (a) surface temperature, (b) sea level, (c) zonal, and (d) meridional pseudo wind stress anomalies.

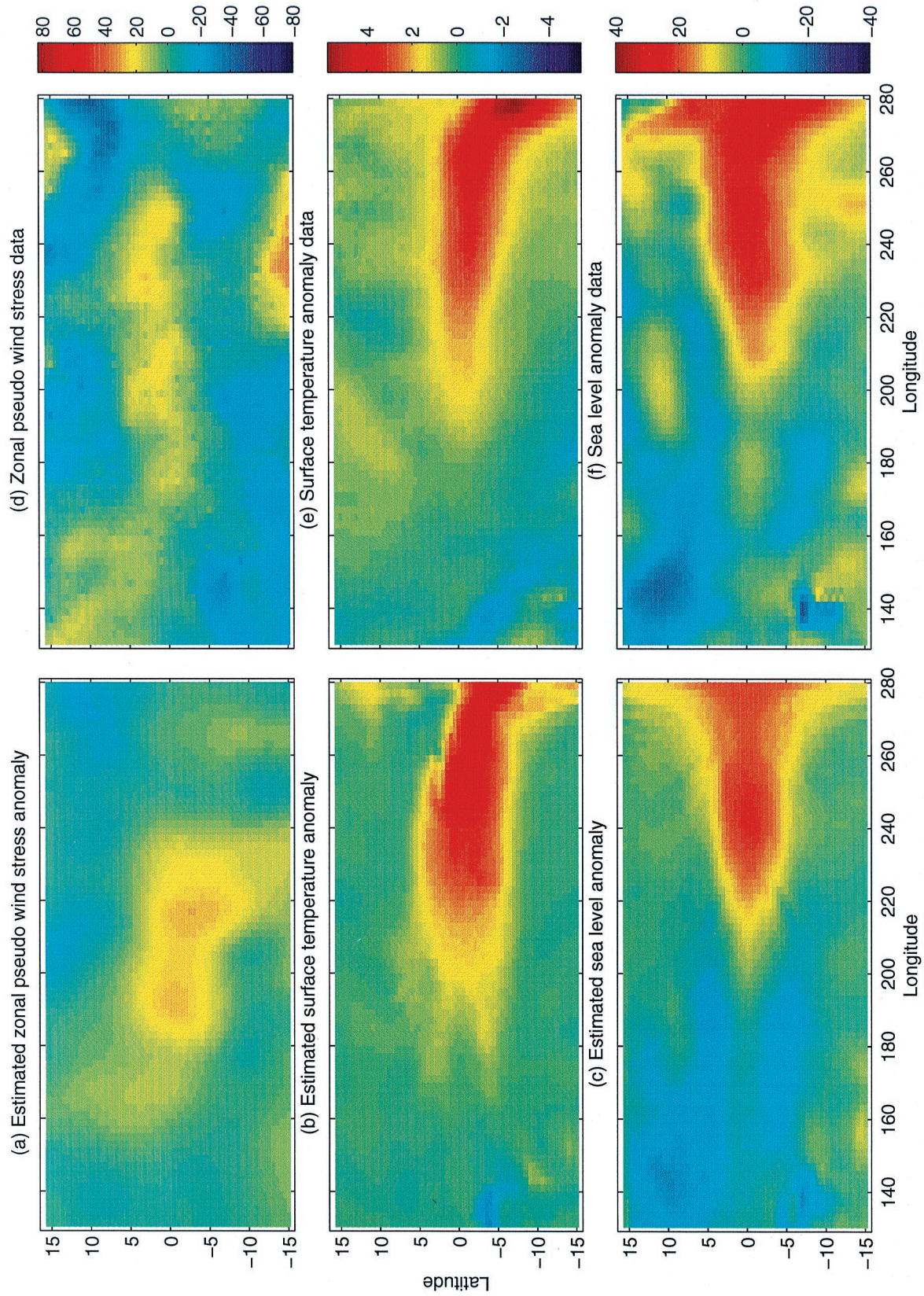


Plate 4. Estimated (a) zonal pseudo wind stress, (b) surface temperature, and (c) sea level anomalies in July 1997 from January 1997 to July 1997 experiment and (d)–(f) the corresponding data.

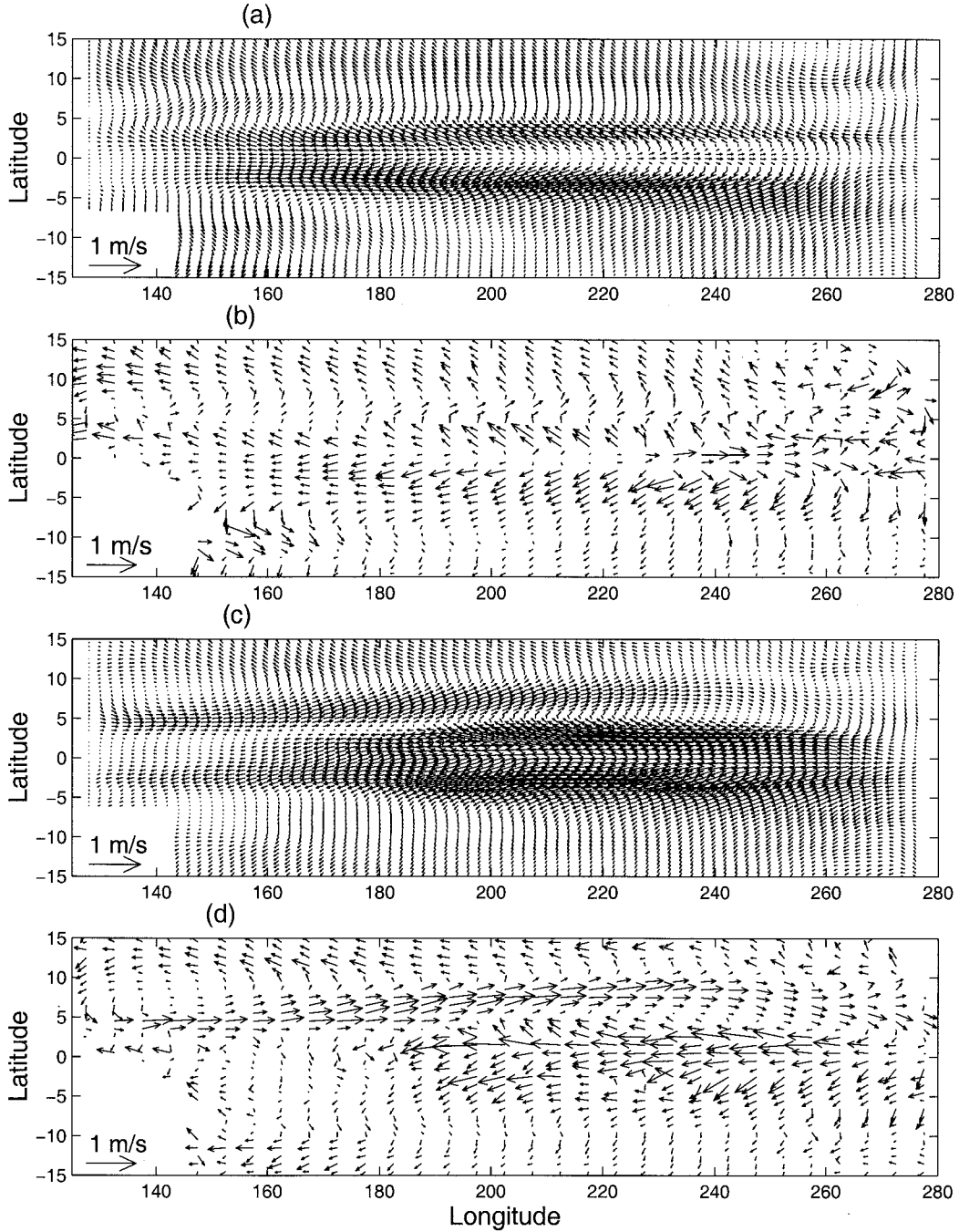


Figure 1. Comparison of model's climatological surface current in (a) and (c) April and October with (b) and (d) Reverdin climatology.

piled by the NOAA Climate Analysis Center. The wind data are zonal and meridional pseudo wind stress compiled by the FSU, also available through the above Web site. Only interannual anomalies of these three types of data are assimilated as our coupled model is an (interannual) anomaly model as described in section 2. The interannual anomalies for SST and pseudo wind stress data are obtained by removing the climatological seasonal cycle averaged between 1980 and 1996 from the full data. Those of SSH are derived by removing the seasonal cycle averaged between October 1992 to October 1996.

4. Assimilation Method

To define the fit of the coupled model to the data, a cost function is formulated to penalize model data misfit in SSHA, SSTA, and wind anomalies during the assimilation period:

$$J = (\mathbf{h}_m - \mathbf{h}_d)^T \mathbf{W}_h (\mathbf{h}_m - \mathbf{h}_d) + (\mathbf{T}_m - \mathbf{T}_d)^T \mathbf{W}_T (\mathbf{T}_m - \mathbf{T}_d) \\ + (\hat{\tau}_m^x - \hat{\tau}_d^x)^T \mathbf{W}_{\hat{\tau}} (\hat{\tau}_m^x - \hat{\tau}_d^x) + (\hat{\tau}_m^y - \hat{\tau}_d^y)^T \mathbf{W}_{\hat{\tau}} (\hat{\tau}_m^y - \hat{\tau}_d^y)$$

where \mathbf{h} , \mathbf{T} , and $\hat{\tau}$ represent vectors of SSHA, SSTA, and PWSA. Different elements in a vector correspond to different

grid points and different months. Subscripts m and d denote model and data. The \mathbf{W} s are weight matrices and ideally should be inversely proportional to the covariance of the measurement error and the representation error (see *Lorenz* [1986] for the latter). Because of the lack of knowledge about temporal and spatial correlations of the errors, the off-diagonal elements are set to zero, i.e., assuming the errors are independent in space and time. The diagonal elements are set to the inverse square of a priori standard errors, being 5 cm for the SSHA, 0.5°C for the SSTA, and $10 \text{ m}^2 \text{ s}^{-2}$ for the PWSA. We seek a solution of the coupled model, which minimizes J by adjusting the control variables. The control variables include the initial conditions and the model parameters.

The initial conditions are initial values of SSTA and components of SSHA and zonal current anomalies within $\pm 15^\circ$ of the equator. Their a priori errors are very difficult to determine (as *Bennett et al.* [1998] reported for the modified *Zebiak and Cane* [1987] model). In our initial attempt, there is no explicit penalty for the deviation of initial conditions from the first guess. However, the penalty of model-data misfit imposed in the first time step of each assimilation experiment provides a stringent constraint to the adjustment of the initial conditions.

Model parameters adjusted are the drag coefficient, frictional timescales for the two baroclinic modes and for the shear layer component, and the relaxation timescale in the SSTA equation. An inequality constraint is implemented to prevent the estimated value to become negative. This is achieved by estimating the squared root of a coefficient. The square of the estimate is then positive. In addition to these coefficients, the rms amplitude ($\sigma_{\frac{1}{2}}^n$ and σ_T^n) of various eigenmodes are also treated as control variables. Adjusting $\sigma_{\frac{1}{2}}^n$ and σ_T^n serves the following main purpose: the original weights for different SVD modes, $\alpha^n = \sigma_{\frac{1}{2}}^n / \sigma_T^n$, describe the contribution of different modes averaged over the time period of the historical data. Adjusting $\sigma_{\frac{1}{2}}^n$ and σ_T^n (and thus α^n), according to the data during the assimilation period, can account for the variation of the relative dominance of different modes (e.g., modes 1 and 2, which reflect the eastern-central and eastern warming, respectively). The adjustments of $\sigma_{\frac{1}{2}}^n$ and σ_T^n and that of the drag coefficient are not redundant to each other. For a fixed time level the former serves to reduce the model-data misfit in PWSA, whereas the latter acts to produce more realistic SSHA and SSTA. The adjustment of a parameter is intended to compensate for model error associated with the value of the parameter. The form of parameterization may present another type of model error (e.g., drag coefficient that is independent of wind speed and linear form of frictions). Parameter estimation can also be used to understand this type of model error.

In principle, the deviation of an estimated parameter from its first guess should be penalized in the cost function to increase the probability of obtaining a unique estimate. Nevertheless, a strong penalty would result in biased estimates if the weights are incorrectly prescribed, whereas a weak penalty has little effect on the estimation. For this initial effort the ranges of model parameters are not explicitly penalized in the cost function, implying that little is known about the errors of the parameters. They are, however, implicitly constrained by the model-data misfits of SSTA, SSHA, and PWSA. The variation of parameter values estimated from data in different periods provides a basis to assess the errors of these parameters, which can be further implemented in the cost function to refine the

estimates. The same applies to the evaluation of a priori errors for initial conditions.

The adjoint method is used to compute the gradient of J with respect to the control variables. The principle of this method is well documented [e.g., *Thacker and Long*, 1988] and so will not be repeated here. The majority of the adjoint code is machine-generated using a software called the Tangent Linear and Adjoint Model Compiler developed by R. Giering [*Giering and Kaminski*, 1998]. The adjoint gradients are used in a preconditioned conjugate gradient algorithm to adjust the control variables iteratively so as to minimize J .

Only data between 15°S and 15°N are assimilated because this is the region of active dynamics, thermodynamics, and coupling in the model, as discussed in section 2. The temporal integration period for each minimization is 6 months. The data constraint is effective only at the middle of each month. The total number of data is roughly twice the total number of control variables for such an integration period. When a 6 month assimilation experiment is completed, a forecast is performed using the end state of the assimilation as initial conditions and using the estimated parameters obtained from the assimilation. In a subsequent experiment the time window is shifted forward by 1 month. The assimilation and forecast procedure are then repeated.

5. Results of the Assimilation Experiment

After 100–200 iterations of the minimization procedure the model-data misfit for SSTA and SSHA are reduced to levels that are close to their a priori errors. However, the estimated zonal PWSA is generally weaker than the observed values. The rms model-data misfits averaged over various 6 month minimization experiments are reduced from the prior values of 8.4 to 4.7 cm for SSHA, 0.93° to 0.46°C for SSTA, 16.8 to $15 \text{ m}^2 \text{ s}^{-2}$ for zonal PWSA, and 11.2 to $10 \text{ m}^2 \text{ s}^{-2}$ for meridional PWSA. Except for zonal PWSA all other quantities agree with the data to within the a priori errors of 5 cm, 0.5°C, and $10 \text{ m}^2 \text{ s}^{-2}$.

To show where these reductions of model-data misfits come from geographically, the spatial distributions of the misfits before and after the data assimilation are shown in Plates 2 and 3. Note that both the simulated and assimilated solutions were obtained in a coupled context. One can think of them as corresponding to the first and last iterations of the optimization, respectively. Therefore they should not be confused with the rms maps between forecasts and observations to be presented in section 6. Before the assimilation, large model-data misfits are seen for (1) SSTA in the eastern equatorial Pacific and off the coast of South America (Plate 2a), and (2) SSHA in the central to eastern equatorial Pacific and the western Pacific between 5° and 10°N (Plate 2b), an area of significant Rossby wave-like activity. These differences are much reduced after the assimilation (Plates 3a and 3b). This demonstrates a reasonable skill of the model in reproducing much of the observed variability in SSTA and SSHA during the 1997–1998 El Niño. The impact of the assimilation is not limited to the equatorial “Kelvin wave” band, but occurs for the off-equatorial “Rossby wave” band in the western Pacific as well. For PWS anomalies, large rms differences from the data exist for both assimilation and simulation. However, the assimilation is closer to data in the equatorial band than the simulation is. For instance, the residual of zonal PWS anomaly between 180° and 220°E near the equator is much smaller for assimilation than for simulation (Plates 2c and 3c). This is important because the zonal

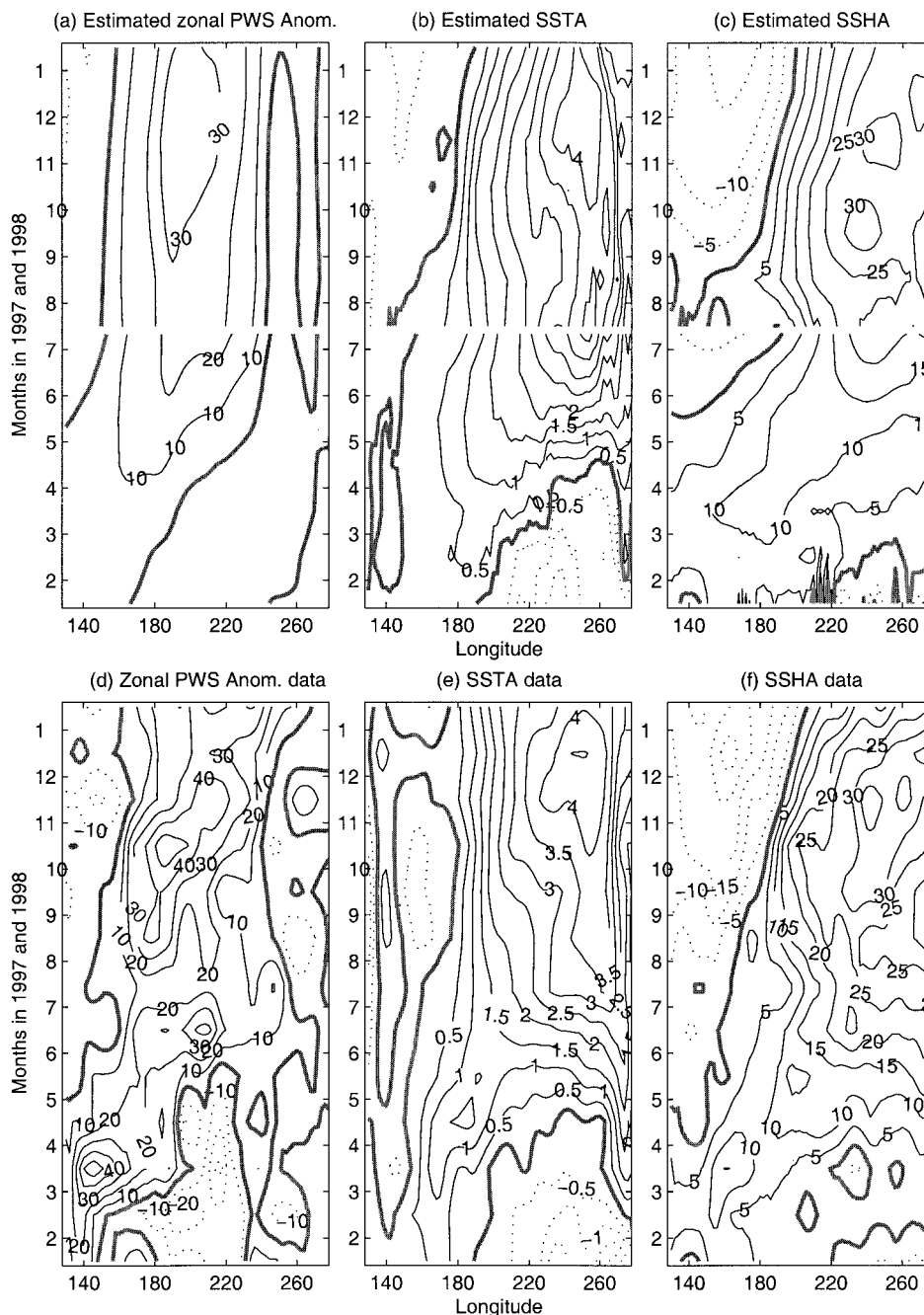


Figure 2. Estimated (a) zonal pseudo wind stress, (b) surface temperature, and (c) sea level anomalies at the equator from two assimilation experiments (January to July 1997 and July 1997 to January 1998) and (d)–(f) the corresponding observations.

wind variability in this area (Plate 1a) is associated with the warming in the central-eastern Pacific. For the meridional PWS the most significant improvement due to the assimilation is the reduction of rms difference in 200°–210°E, 7°–15°N.

To illustrate the temporal evolution of the estimated fields, the longitude-time structure of the estimated equatorial zonal PWSA, SSTA, and SSHA for two consecutive experiments (January to July 1997 and July 1997 to January 1998) presented in Figures 2a–2c in comparison with the data shown in Figures 2d–2f. The dominant temporal variations in the estimated fields resemble the observations reasonably well.

The estimated zonal PWSA is smoother and overall weaker

than the observed values. The westerly wind bursts in the western Pacific were not recovered because the SVDs, a low-passed filter in nature, cannot reproduce these transient features. The gradual buildup of westerly wind anomaly in the western and central Pacific in early 1997 was captured but with a weaker intensity than the data. Consequently, the estimated anomalous warming in the western to central Pacific is weaker than the observation. The anomalous warming in the eastern Pacific (near the model's eastern boundary) is also weaker than the observed strength.

Selected estimated fields from the two aforementioned assimilation experiments, corresponding to July 15, 1997, and

December 15, 1997, are shown in Plates 4 and 5 in comparison with the corresponding data. The dominant spatial patterns of the estimated fields are very similar to the data. The differences mostly appear in the strength and to some degree in the spatial extent of the patterns. The most notable difference is in the PWSA.

The improvements in the assimilation products are due to (1) the correction of initial condition, which results in better agreement with data, and (2) the adjustment of model parameters, which regulates the balance between forcing and damping in the ocean component and thus the strength of the coupling. The following discussion elucidates point 2, which is not as intuitive as point 1.

Table 1 shows the estimates of the model parameters for various 6 month assimilations. The estimated drag coefficient is generally larger, corresponding to an enhanced coupling strength and larger forcing for the ocean component. The estimated baroclinic frictional timescales and relaxation timescale for SSTA are generally longer than their corresponding prior values, resulting in weaker damping. These adjustments reflect the data constraint that requires the model to reproduce the rapid development of the large-amplitude warming event. In the coupled model the drag coefficient and the damping coefficients affect the strength of forcing and damping of an oceanic anomaly. This, in turn, affects the coupled evolution of the anomaly. Therefore the estimated coefficients contribute significantly to the improved development of the warming event in the assimilation product.

The difference in the values of parameters for various experiments is relatively large. One possible cause is estimation error due to the mutual compensation between the forcing and damping constants. For example, the three experiments covering the periods of February to August 1997, March to September 1997, and April to October 1997 have relatively small drag coefficients (weaker forcing) and relatively long baroclinic and SSTA damping timescales (weaker damping). The opposite tendency is found for the first three experiments (large drag coefficients and short damping timescales). To reduce these compensations, one needs to determine the error of each parameter accurately and use it to impose an explicit penalty for the parameter in the cost function. The variation of parameters found in this initial attempt is helpful in choosing suitable errors for a refined estimation.

Variation in the estimated parameters may also reflect the limitation in the form of the parameterization. In principle, the drag coefficient should vary in space and time depending on wind speed and air-sea temperature difference [Trenberth *et al.*, 1989]. A constant drag coefficient would absorb this dependence by changing the constant itself. The same is true for the damping coefficients. Dissipation in the real ocean depends on the flow field in a far more complicated way than through a linear form with a constant coefficient. The unresolved physics that the parameterization intends to parameterize could vary in space and time and is thus not accounted for by a constant coefficient.

The difference between the prior and the averaged estimate for the drag coefficient, 1.20×10^{-3} versus 1.55×10^{-3} , is smaller than the scatter among various observations discussed by Large and Pond [1981]. It is also within the range of analysis errors considered by Trenberth *et al.* [1989] if space-time variations are taken into account. The difference between the prior and the averaged estimates for the baroclinic damping timescales is fairly large (12 and 6 months versus 60 and 30 months

for the two vertical modes, respectively). The value of 12 months was chosen primarily on the basis of previous experience for forced ocean models with only one vertical mode to reproduce the overall sea level variability over periods where ENSO events are not as strong. The values estimated here are based on a coupled model with two vertical mode fitted to three types of data over a short period where the magnitude of the anomalous state is unprecedented. In addition to the differences between forced and coupled models, a two-mode ocean model does not necessarily share the same damping coefficient as that with only one mode for the following reasons. The frictional constant is meant to “parameterize” the contributions from some unresolved physics. These contributions are model-dependent (apart from being space- and time-dependent). A model with more complete physics needs less contribution from the unresolved physics (i.e., a reduction in the value of the “damping” constant). The second vertical mode includes some physics not represented by the one-mode model. Therefore the reduction of damping constant (less contribution from unresolved physics) is not unreasonable. The above rationale is somewhat analogous to ocean general circulation model (OGCM) mixing coefficients, which should decrease if the physics that explicitly describe the mixing processes is included or as the resolution increases.

It is also important to emphasize that we are not suggesting that the values of the parameters estimated from the data during the warming phase of the 1997–1998 event be used as climatological values to simulate the overall variability in previous data. None of the previous events match the unprecedented magnitude of the current one. In fact, our on-going work on fitting the model to observations in the early 1990s generally results in damping timescales that are shorter than the present estimates (somewhat similar to the first two experiments as listed in Table 1). Those results will be reported in a separate paper along with an application of the assimilation procedure to the data in the 1980s. A relatively long damping timescale of 30 months was used in the Zebiak and Cane [1987] model for all conditions. Because of possible model dependence, we cannot comment on whether this timescale would produce a more realistic state during 1997 than a shorter timescale would for that model.

Apart from the forcing and damping coefficients, the (rms) amplitude of various eigenmodes for SSTA and PWSA is also adjusted during the assimilation (see section 4). Thus the weights for different SVD modes, $\alpha^n = \sigma_2^n / \sigma_7^n$, are modified to allow a better fit of the model state to the data. The adjustment of α^n is much smaller than the adjustments of the drag and damping coefficients. On average, α^n increases by 1, 4, 14, and -21% for modes 1–4, respectively (negative means decrease). The variation of the changes among various experiments is relatively large (50–100%) because of estimation errors associated with mutual compensation (similar to that for the drag and damping coefficients). This variation precludes the possibility of examining the relative role of different modes among different experiments. However, the signs of the mean values are consistent with the improved model fit to the data as described below. As discussed in section 2, modes 1 and 2 (Plate 1) describe the eastern-central and eastern warming patterns, respectively; mode 3 also appears to contribute to warming near the eastern boundary. The 1997–1998 El Niño resembles a classical one (e.g., the 1982 El Niño) in many aspects but with more intense warming in the eastern-central and eastern equatorial Pacific. Therefore the consistent in-

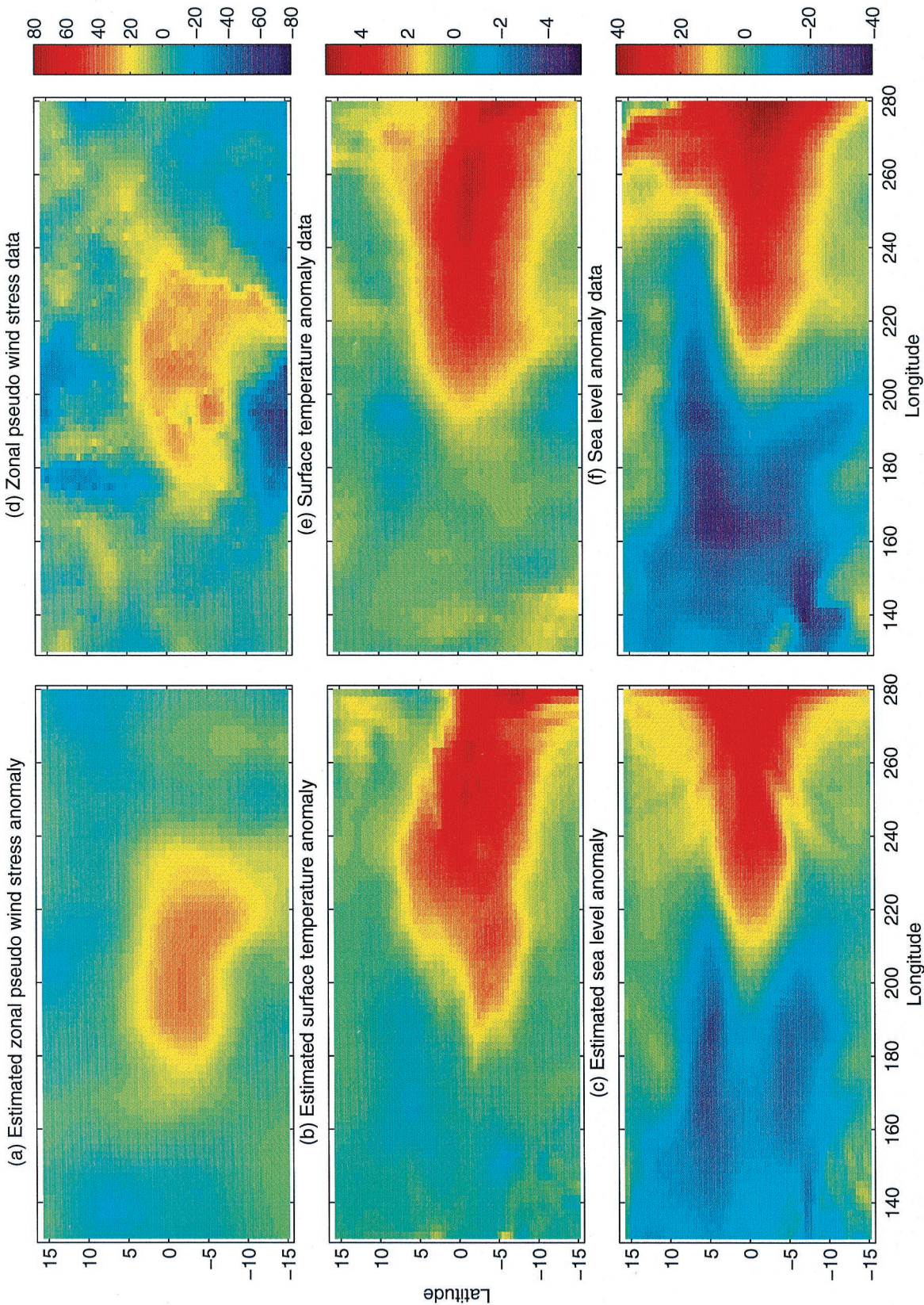


Plate 5. Estimated (a) zonal pseudo wind stress, (b) surface temperature, and (c) sea level anomalies in December 1997 from July 1997 to January 1998 experiment and (d)–(f) the corresponding data.

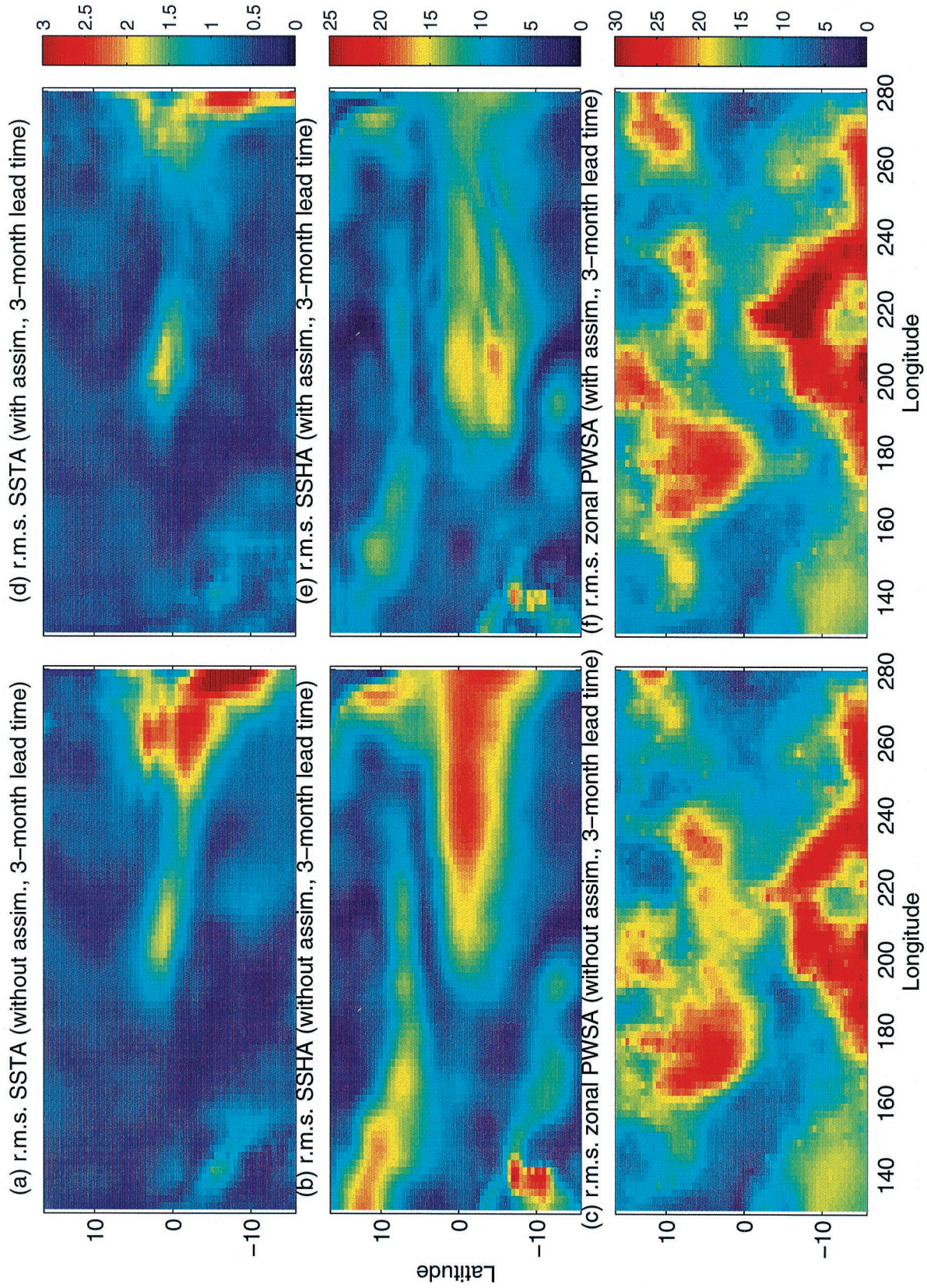


Plate 6. Rms misfits between forecasts with a 3 month lead time and the data: forecasts (a)–(c) without and (d)–(f) with data assimilation before the prediction for surface temperature, sea level, and zonal pseudo wind stress anomalies.

Table 1. Parameters Estimated From Various Assimilation Experiments^a

	Drag Coefficient ($\times 10^{-3}$)	Baroclinic Frictional Timescale (Mode 1), months	Baroclinic Frictional Timescale (Mode 2), months	Ekman Frictional Timescale, days	Surface Temperature Anomaly Damping Timescale, days
Sept. 1996 to March 1997	1.57	21	10	5.24	120
Oct. 1996 to April 1997	1.58	27	13	5.48	120
Nov. 1996 to May 1997	1.55	40	21	2.93	152
Dec. 1996 to June 1997	1.50	71	50	0.57	218
Jan. 1997 to July 1997	1.56	80	47	0.50	198
Feb. 1997 to Aug. 1997	1.30	102	45	0.51	232
March 1997 to Sept. 1997	1.40	110	27	0.50	181
April 1997 to Oct. 1997	1.45	84	54	0.52	215
May 1997 to Nov. 1997	1.62	51	27	0.54	151
June 1997 to Dec. 1997	1.77	47	25	0.25	131
July 1997 to Jan. 1998	1.75	37	20	0.51	136
Average for various experiments	1.55	61	31	1.59	168
Prior values	1.2	12	6	2.0	125

^aBaroclinic frictional timescales are rounded to the nearest integer month, and surface temperature anomaly damping timescales are rounded to the nearest day. The averaged values over various experiments and the prior values are also listed.

creased weights for modes 1–3 reflect the need to enhance the contributions from these modes to account for the unprecedented magnitude of this El Niño. In particular, the enhanced mode 3 seems to help produce a significant warming near the eastern boundary from 0° to 10°S (e.g., Figure 2b), which significantly reduced the model-data misfit in that region (Plates 2a and 3a). The reduction of the weight for mode 4 is somewhat obscured because of the lack of evidence to tie this mode directly to a physical feature. One may argue that this mode does not represent the dominant signal of a classical El Niño and is thus down-weighted. These sensible adjustments underline the potential usefulness of adjusting the weights of different modes computed from historical data using several types of current data.

6. Forecast Experiment Based on Assimilation Products

The assimilation products presented in section 5 are used to initialize forecasts. The ocean state at the end of a 6 month assimilation serves as the initial state. Parameters estimated during the assimilation period are used for the forecast. Thus the model states during the assimilation and the forecast periods belong to the same coupled model trajectory. This eliminates the initial shock of a forecast caused by the inconsistency of the initial state with coupled model physics.

In order to evaluate the quality of the forecasts, several regions are selected in which a spatially averaged variable, or index, is examined. These regions include Niño3 (central-eastern equatorial Pacific 210°–270°E and 5°S–5°N, area of large SSTA and SSHA), Niño4 (western-central equatorial Pacific 160°–210°E and 5°S–5°N, an area of large zonal PWS variability), Niño6 (northwestern tropical Pacific 140°–180°E and 2°–10°N, an area of large SSHA associated with Rossby wave-like variability), and Niño7 (north-central tropical Pacific 200°–240°E and 2°–10°N, an area of large meridional PWS variability).

The predicted Niño3 index for SSTA, Niño3 and Niño6 indices for SSHA, Niño4 index for zonal PWS, and Niño7 index for meridional PWS resulting from forecasts initialized

from the assimilation products are shown in Figures 3a–3e. The counterparts derived from forecasts simply initialized from the ocean states forced by “statistical wind” (see section 2) with default parameters are shown in Figures 3f–3j. With data assimilation in the initialization phase (optimal initialization), improvement is seen in the following aspects: (1) the magnitude of the anomalies are larger and closer to the observed ones, (2) the time of the peak warming is close to December 1997 as observed (forecasts without optimal initialization always peak slightly after the initialization), and (3) the evolution of the anomalous state from the warming to the initial decay phase is more consistent with the data. Judging from Niño3 SSTA, a commonly presented index from various ENSO forecast models, the present system can predict a larger amplitude of SSTA for this warming event than most statistical based hindcasts/forecasts and is close to many forecasts based on much more complicated models, some also with data assimilation in the initialization phase.

Even with optimal initialization, the forecast significantly underestimated the magnitude of the warming if starting before, say, May 1997. This seems to be caused by the underestimate of the strength of the westerly wind stress anomaly, which emerged in late 1996 and evolved through the spring of 1997 (the statistical atmosphere cannot represent these features). However, from late spring and early summer of 1997 the model (with optimal initialization) reasonably reproduced the rapid development of the observed warming, its amplitude and phase, and its initial decay.

To examine the temporal evolution along the equator, variables predicted by forecasts initialized in March 1997, with and without data assimilation prior to the forecast (optimal initialization), are presented in Figure 4 together with the corresponding observations. Note that the contour intervals for the forecasts are half of those for the observations. The forecast without optimal initialization failed to show any significant warming. That with optimal initialization predicted a warming over 2°C in the central-eastern Pacific with a peak time that agrees with the data (December 1997). The pool of maximum warming is too narrow and somewhat too westward compared

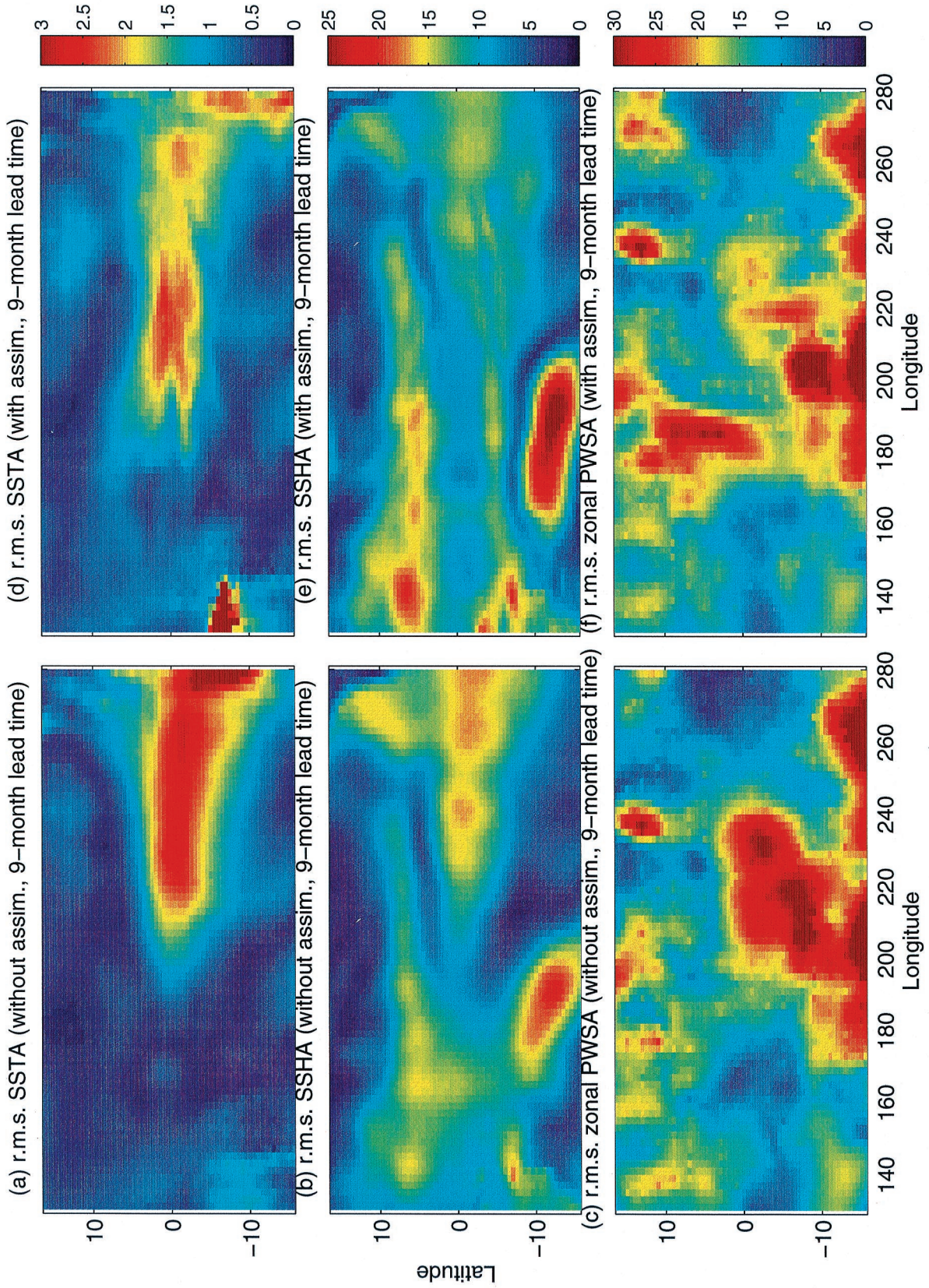


Plate 7. Rms misfits between forecasts with a 9 month lead time and the data: forecasts (a)–(c) without and (d)–(f) with data assimilation before the prediction for surface temperature, sea level, and zonal pseudo wind stress anomalies.

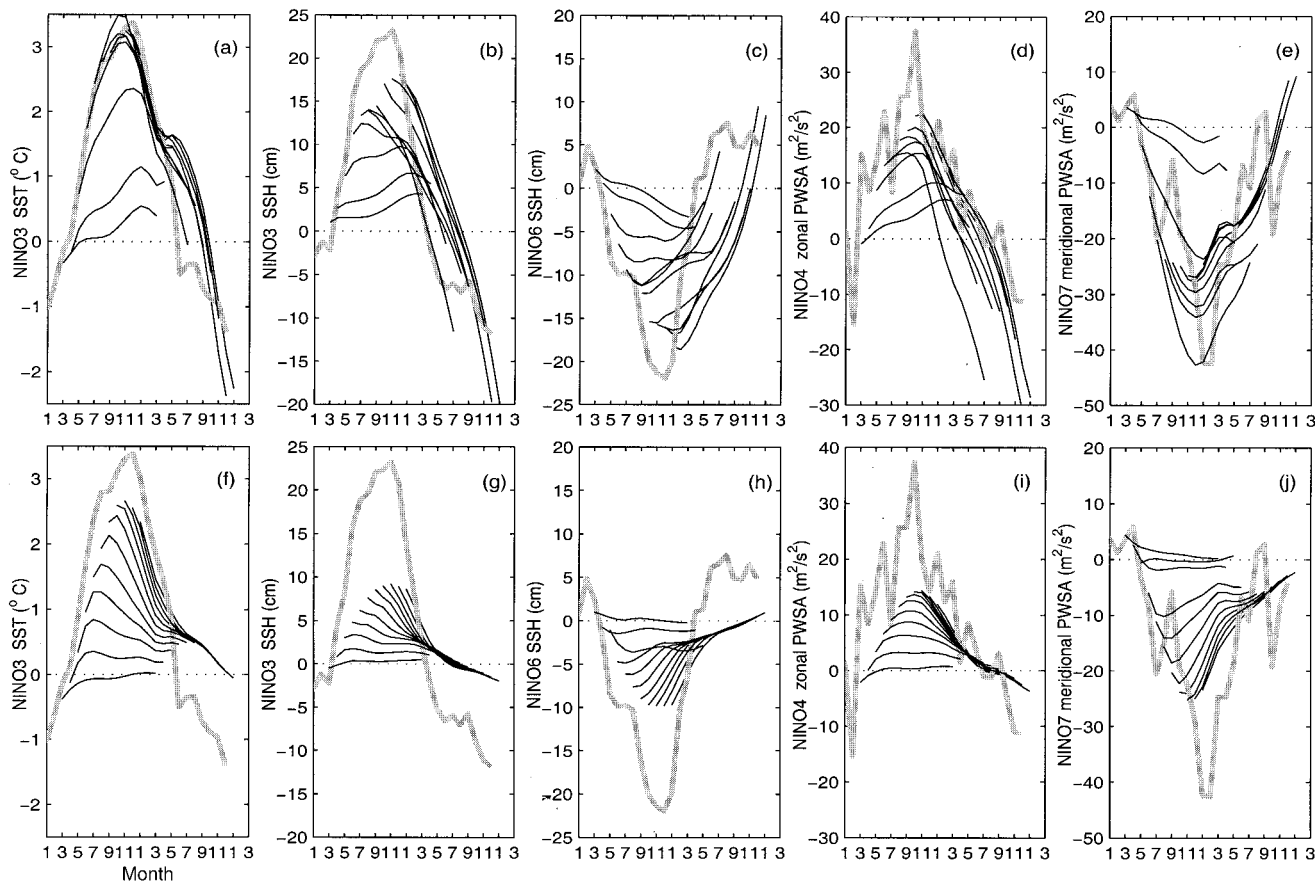


Figure 3. Forecasted indices Niño3 SSTA, Niño3 SSHA, Niño6 SSHA, Niño4 zonal PWSA, and Niño7 meridional PWSA: (a)–(e) forecasts with and (f)–(j) without data assimilation in the initialization phase. Shaded curves represent data (see text for definitions of indices).

to the data. This is related to the narrow longitudinal extent of the predicted maximum PWSA. Figure 5 shows another case where the forecasts are initialized in July 1997. By this time the forecast with optimal initialization is able to predict an anomalous warming that is close to the observed magnitude.

An unsatisfactory aspect in the forecast after the peak warming is the delayed transition from warm to normal condition in the Niño3 area during the late spring of 1998 (Figures 3a and 3f). The observed abrupt switch from warm to cold condition east of the dateline (Figure 5h) was not captured by the model regardless of the initialization method. The observed easterly wind burst in May 1998 in the western Pacific (Figure 5g) may have contributed to this sudden transition. The inability to predict these easterly wind burst in almost all forecast models might be a major cause for the failure to predict the abrupt transition.

Unlike in the Niño3 region, the transition from warm to cold condition in the central equatorial Pacific (Niño4 region) is premature for the forecasts: it occurred in early 1998 rather than in May–June 1998 as observed (Figures 5b and 5h). Associated with this premature cooling is an easterly wind anomaly near the dateline (Figures 5a and 5d), which is not supported by observation (Figure 5g). Again, optimal initialization did not cause the premature cooling and related easterly because these features appear in forecasts with and without optimal initialization. However, the magnitude of the cooling is enhanced by the optimal initialization. This is a result of the

relatively symmetric nature of the statistical atmosphere with respect to positive and negative anomalies: if the model is fitted to a large-amplitude warming event (during the assimilation period), it would evolve into a large-amplitude cooling event (during the forecast). Reproducing the asymmetry of El Niño and La Niña events remains to be a challenge to this class of models.

The overall impact of optimal initialization on forecasts are further illustrated by the rms deviations of predicted variables from the corresponding observations in Plates 6 (3 month lead time) and 7 (9 month lead time). Plates 6a–6c and 7a–7c are for forecasts without optimal initialization, and Figures 6d–6f and 7d–7f are for forecasts with optimal initialization. The differences in rms deviations from the data with and without optimal initialization are shown in Plate 8 (negative values indicate improvement). The observed rms variations are shown in Plate 9 for reference. Consistent improvement (reduction in rms deviation from the data) is found for SSTA and SSHA in the central-eastern Pacific Niño3 area and zonal PWSA in the central Pacific. Averaged over lead times of 1–12 months (not shown), the reduction in rms deviation is 0.5–1°C for SSTA and 4–7 cm for SSHA in the central-eastern equatorial Pacific and 5–10 $\text{m}^2 \text{s}^{-1}$ for zonal PWSA in the central Pacific. The improvement is larger than the prior errors for SSTA and SSHA used during the assimilation.

In the western-tropical Pacific between 2° and 10°N (the “Rossby wave band”), improvement is clearly seen for SSHA

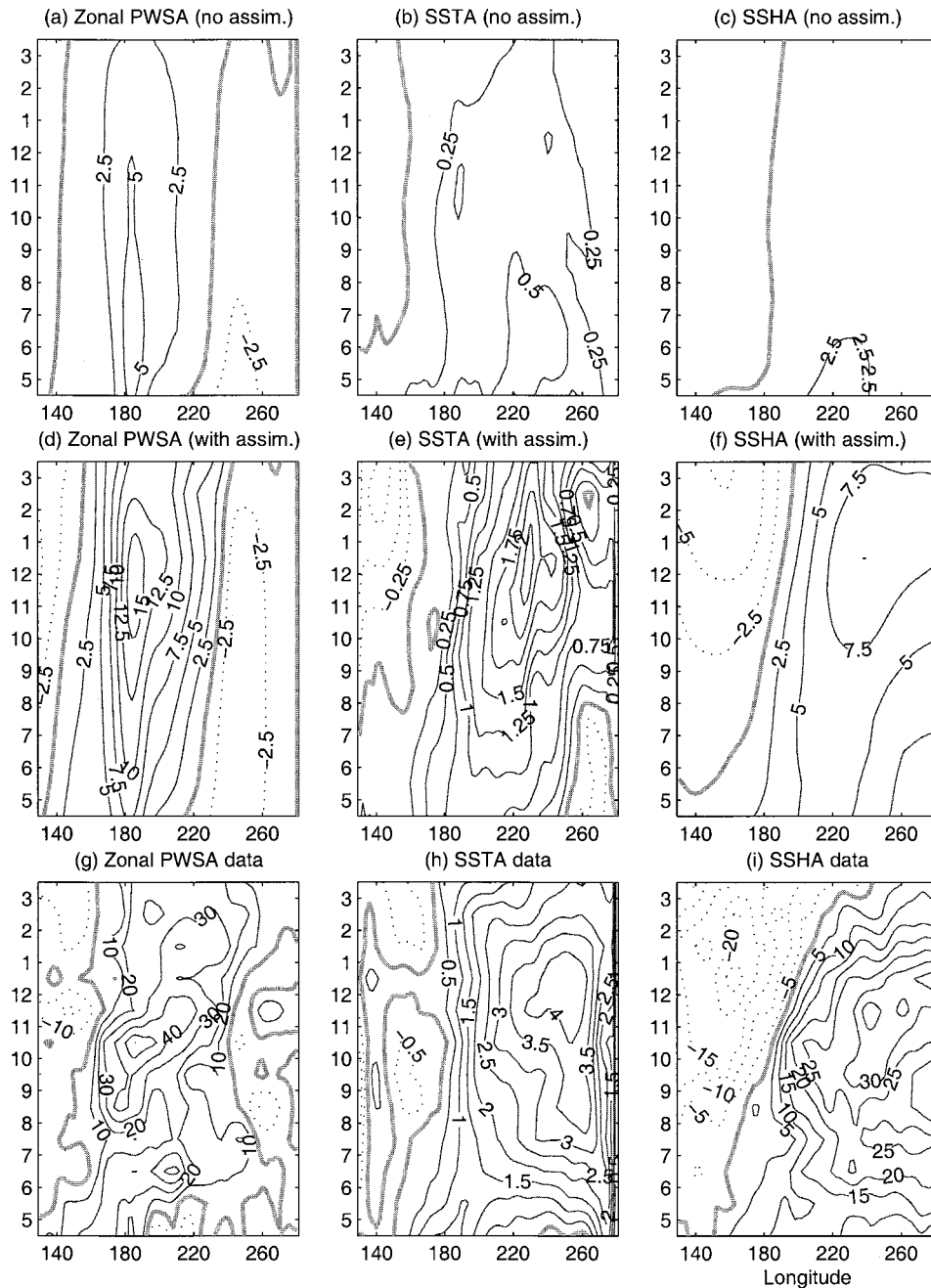


Figure 4. Predicted and observed longitude-time distribution of zonal pseudo wind stress, surface temperature, and sea level anomalies at the equator. The predictions are obtained from forecasts starting in March 1997.

for shorter lead times (Plates 6b, 6e, and 8b). For longer lead times, however, the rms deviation of SSHA is actually larger for forecasts with optimal initialization (Plate 7b, 7e, and 8e). Figures 3c and 3h (the averaged SSHA in the Niño6 area) illustrate the cause for this increase in rms deviation. The predicted magnitude of the negative SSHA is larger and more realistic than that without optimal initialization. Nevertheless, the predicted transition from negative anomaly to normal condition is delayed compared to the data. The larger amplitude of SSHA resulting from optimal initialization, when offset in time from the data, results in relatively large rms deviation from the data. Actually, the predicted SSHA without optimal initialization returns to the normal state even later (November

1998; see Figure 3h). The reason for the smaller rms deviation without optimal forecast is because the predicted SSHA is very small throughout. Similar to the delayed cooling in the Niño3 area and premature cooling in the Niño4 area, the delayed transition of negative SSHA to normal condition in this band is not caused by optimal initialization because it exists in the forecast without optimal initialization as well.

For longer lead times, SSTA near 180°–210°E and zonal PWSA near 180°E have larger rms deviations for forecasts with optimal initialization. This is a result of the premature cooling and easterly discussed earlier (referenced to Figure 5), which exists in forecasts with and without optimal initialization but is enhanced in magnitude by the optimal initialization.

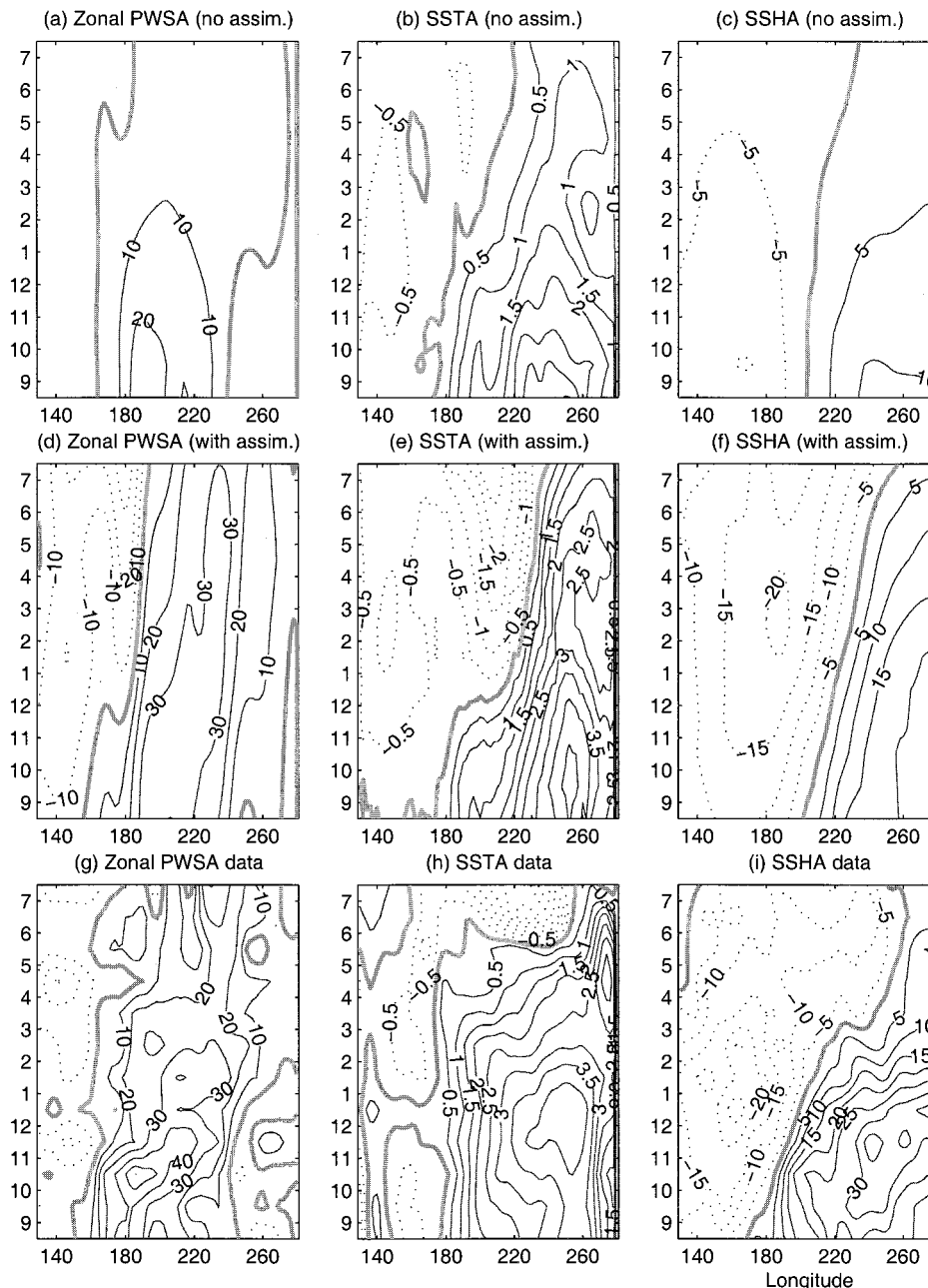


Figure 5. Predicted and observed longitude-time distribution of zonal pseudo wind stress, surface, temperature, and sea level anomalies at the equator. The predictions are obtained from forecasts starting in July 1997.

Another means of illustrating the impact of data assimilation on forecasts is through spatial maps of temporal correlation of predicted variables with the corresponding observations (Figure 6) and the differences in correlations with and without optimal initialization (Figure 7). Optimal initialization results in improved correlations by ~ 0.2 in most parts of the equatorial region for SSTA and SSHA and in the central equatorial Pacific for zonal PWSA. The improvement of 0.2 is close to the 95% significant level of the correlation values and is thus marginally significant. It is worth noting that optimal initialization improves the correlation in the central equatorial Pacific, although the rms deviation from data is larger (Plate 8d). Therefore, despite the large and premature cooling in the central equatorial Pacific at longer lead times the overall ten-

dependency of the predicted SSTA in that region is not degraded by optimal initialization.

Like the assimilation, these improvements are due to the combined effect of (1) the dynamically consistent initial state that is close to observations and (2) parameters that are determined from several types of observations preceding the forecasts. The improved initial state has a larger impact on prediction in short lead time (the first few months). The estimated parameters properly set the relative strength of forcing and damping. This allows the anomalous model state to evolve, in longer lead time, into a large warming event that has a more realistic peak timing and amplitude in contrast to the prior parameters with which the anomalous model state is damped out quickly.

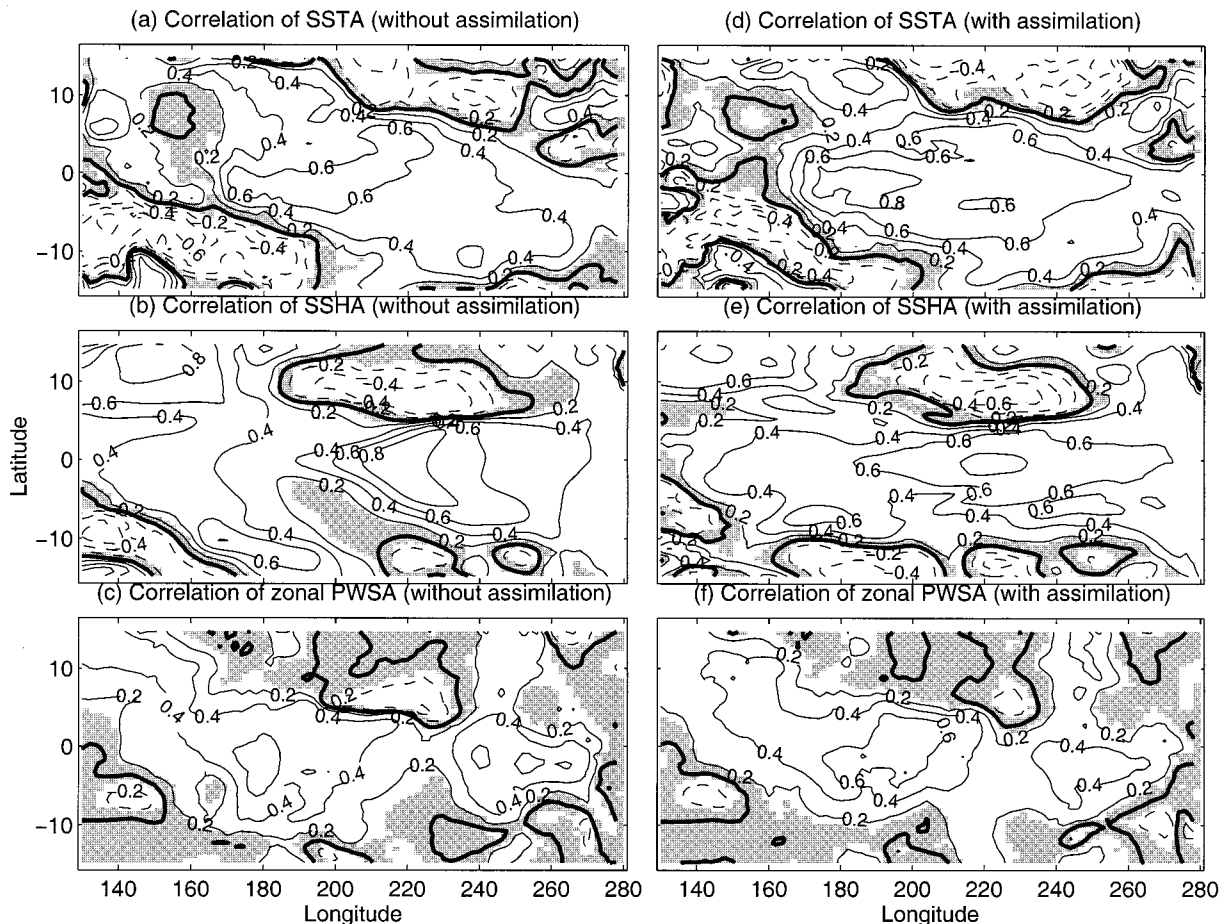


Figure 6. Correlations between forecasts and the data: forecasts (a)–(c) without and (d)–(f) with data assimilation before the prediction for surface temperature, sea level, and zonal pseudo wind stress anomalies. Shaded areas indicate insignificant correlations.

7. Discussion: Parameter Estimation

In sections 5 and 6 we mentioned the role of parameter estimation during the assimilation and its impact on forecast. In summary, the assimilations generally result in larger drag coefficients and smaller damping coefficients (baroclinic friction and SSTA relaxation constant) than their corresponding prior values. The combination of these adjustments enhances the strength of wind forcing and reduces the damping in the ocean component and thus allows the coupled model to fit the data better during the assimilation and to develop a large-amplitude warming anomaly during the forecast. In this section, the role of parameter estimation is further evaluated.

As an example to illustrate the individual role of various parameters and their combined effect, Plate 10a shows the estimated Niño3 SSTA resulting from the experiment during December 1996 to June 1997 and those obtained by turning off the adjustment of various parameters one by one as well as simultaneously, keeping the estimated initial state unchanged. Turning off the adjustment of any of these parameters is seen to decrease the model's skill in reproducing the rapid development of SSTA. When the solutions are integrated forward into the forecast period (Plate 10b), the impact of resetting the estimated parameters to prior values is even more significant. Therefore the optimal adjustment of the drag coefficient, baroclinic frictions, and SSTA relaxation constant all contribute

positively toward the model's improved ability to evolve into a large-amplitude warming event. Yet the combined effect of various parameter adjustments has the largest impact.

In a recent study, *Bennett et al.* [1998] fitted 1 year's worth (April 1994 to March 1995) of monthly mean anomaly of Reynolds' SST, Z20 (depth of the 20°C isotherm, the approximate thermocline depth) and surface wind velocities from the TAO measurements to a modified *Zebiak and Cane* [1987] model using both a weak and a strong constraint formulation. In the weak constraint case, deviation from model dynamics is allowed subject to a dynamical misfit penalty in the cost function in addition to model-data misfit. In the former formulation the fit to the data is largely within assumed standard errors of data (0.3°C, 3 m, and 0.5 m s⁻¹ for anomaly SST, Z20, and surface wind velocity, respectively), but the dynamical misfit is larger than the estimated standard errors of dynamics. In the latter formulation, where model dynamics were assumed "perfect" (equivalent to the adjoint formulation with all the model errors attributed to initial state only), the estimated spatial structure of SSTA bears little resemblance to that in the data; the estimated Z20 and wind velocity are even more "unrecognizable."

Our findings do not contradict those of *Bennett et al.* [1998] for several reasons: (1) We not only adjust initial conditions but model parameters as well. The latter partially compensates

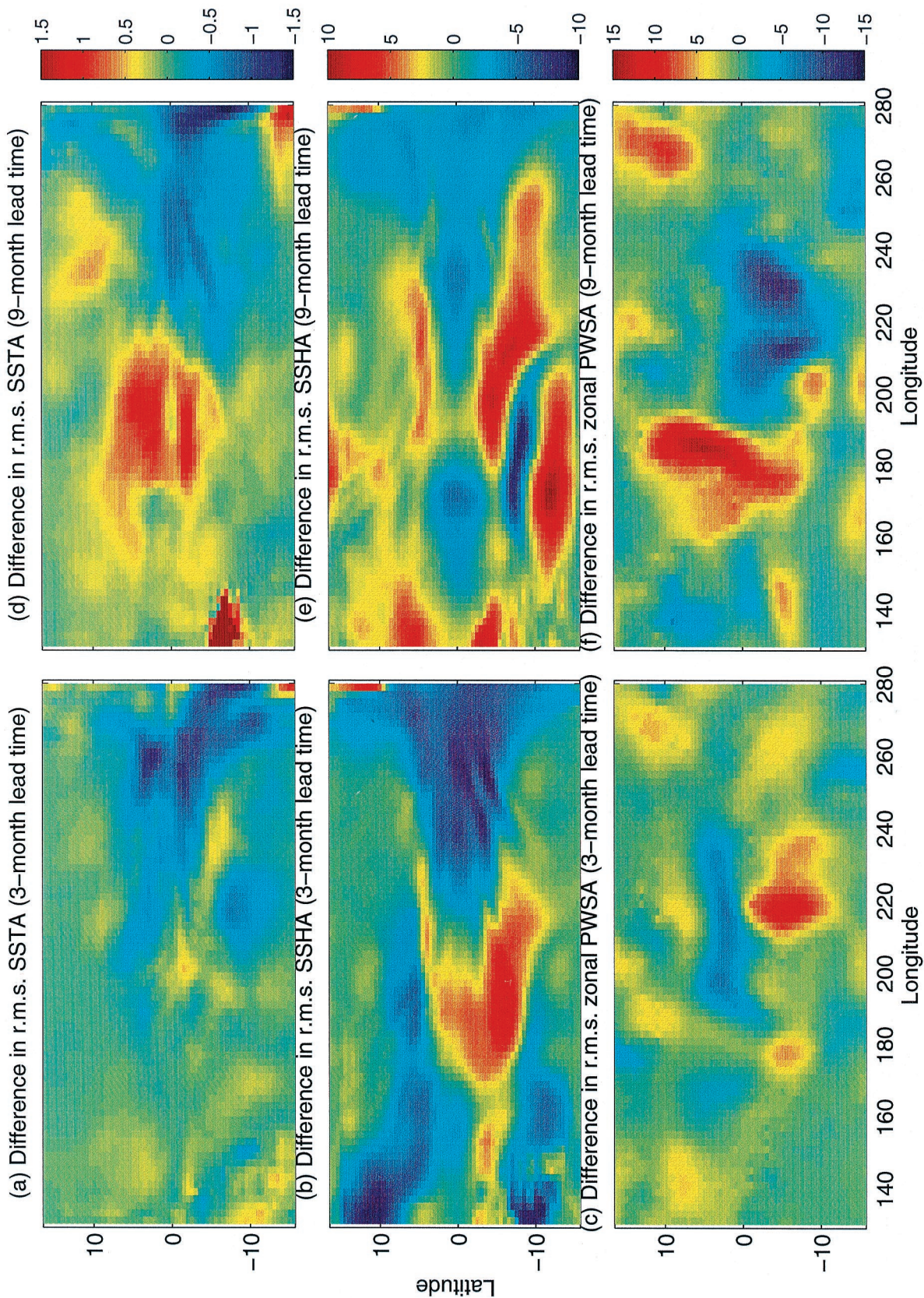


Plate 8. Differences of rms misfits with and without data assimilation before the prediction for a lead time of (a)–(c) 3 and (d)–(f) 9 months for surface temperature, sea level, and zonal pseudo wind stress anomalies.

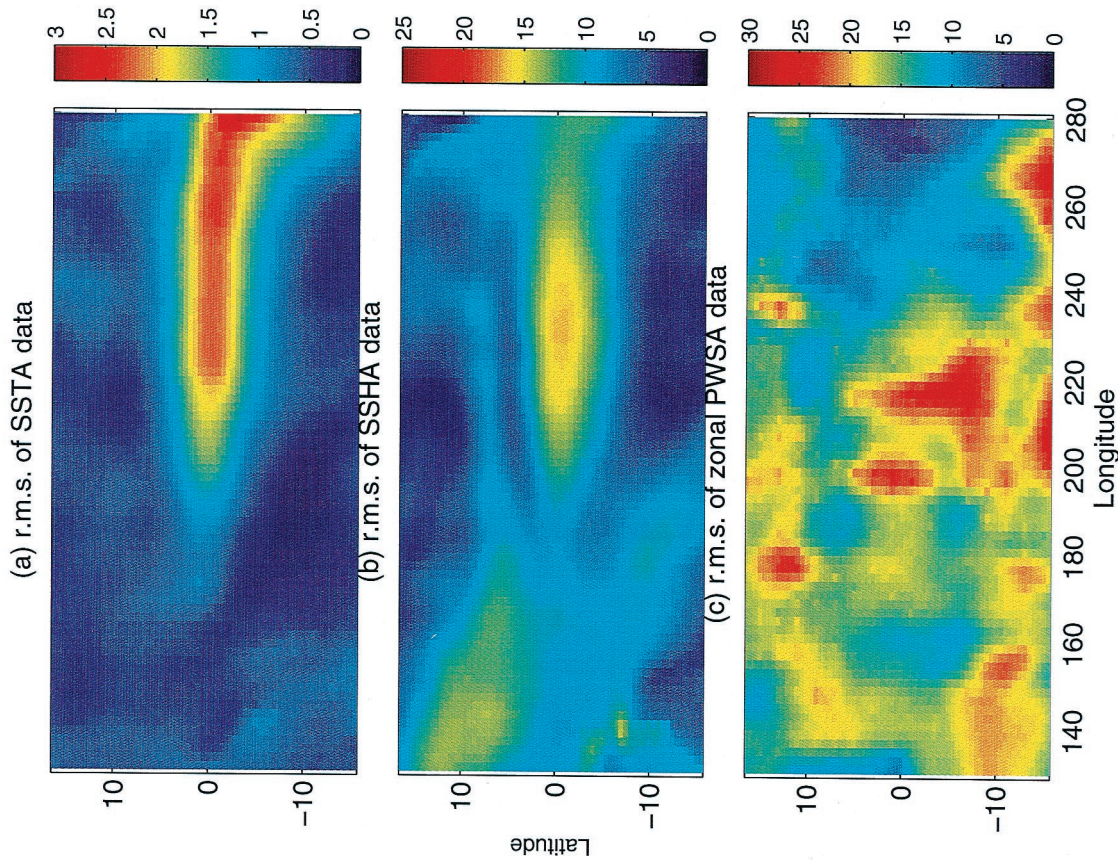


Plate 9. Rms variation of the observed (a) surface temperature, (b) sea level, and (c) zonal pseudo wind stress anomalies during the period of study (September 1996 to December 1998).

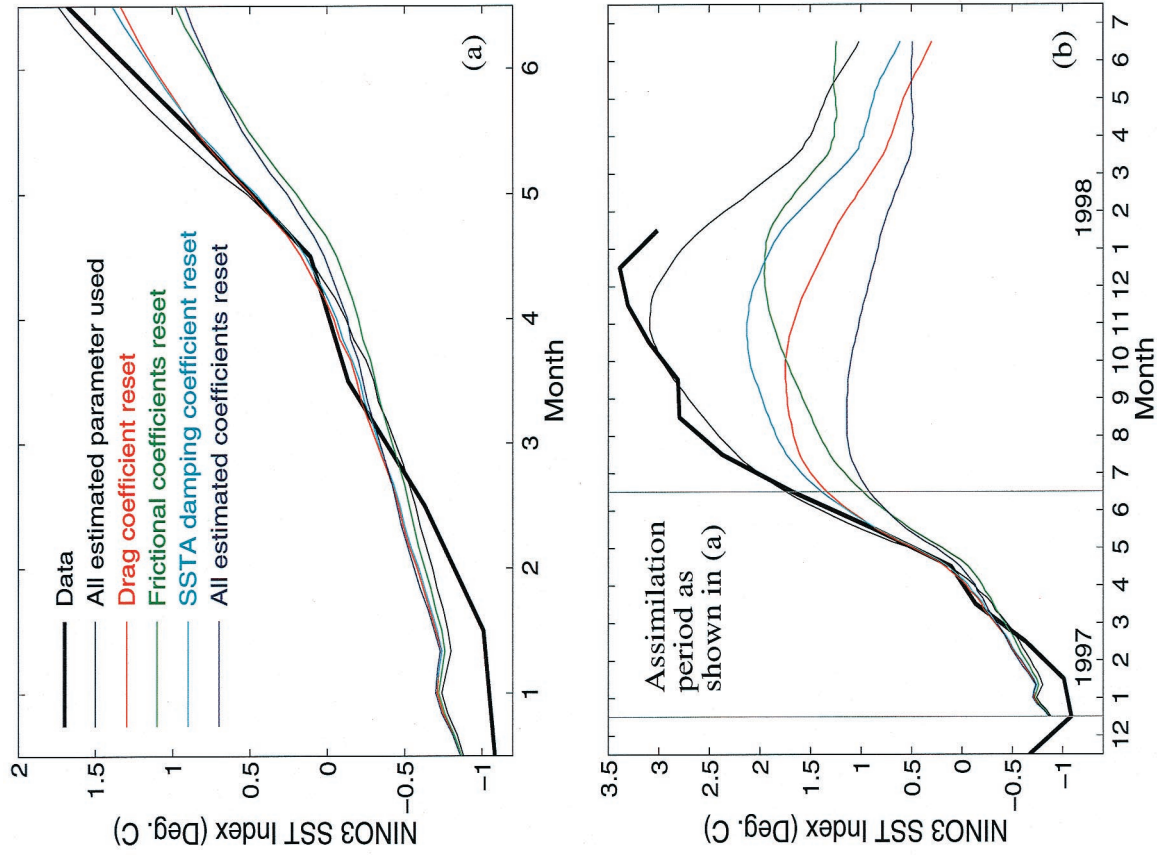


Plate 10. (a) Estimated Niño3 SST from December 1996 to June 1997 and subsequent forecast using all estimated parameters (thin black) and with various parameters reset to prior values (red to blue). (b) Extension of the solutions in Plate 10a forward for another year.

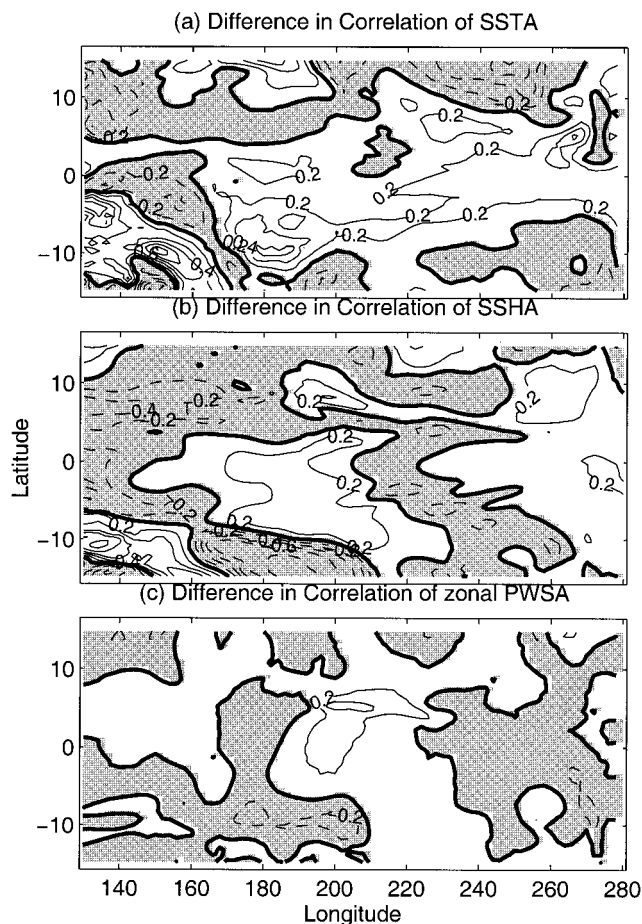


Figure 7. Differences of correlations with and without data assimilation before the prediction for surface temperature, sea level, and zonal pseudo wind stress anomalies.

for some model errors. We have performed experiments by adjusting initial conditions only. Understandably, the resultant fits deviate from the data more than the case where parameters are adjusted. An example is shown in Plate 11 in which the estimated SSHA in July 1997 with only initial state adjusted compares poorer to the data than that with both initial state and parameters adjusted. (2) Coupled models are often sensitive to small changes in parameters and numerics, let alone difference in physics. Our coupled model is sufficiently different from the modified *Zebiak and Cane* [1987] model that the skill of fitting the data could be different. (3) The data errors used by *Bennett et al.* [1998] are smaller than those adopted here: for example, 0.3°C versus 0.5°C for SSTA and 0.5 m s^{-1} versus about 3.33 m s^{-1} (squared root of $10\text{ m}^2\text{ s}^{-1}$) for wind speed. The values used by *Bennett et al.* [1987] were considered to be measurement errors only, whereas the ones we used were meant to include some model errors.

8. Concluding Remarks

Sea level, surface temperature, and pseudo wind stress anomaly data during the 1997–1998 El Niño are assimilated into an intermediate coupled model of the tropical Pacific over various 6 month periods. Model-data misfits are minimized by optimally adjusting initial state and model parameters using the adjoint method. With these adjustments the coupled model

is found to have a reasonable skill in reproducing observed interannual variability of SST and sea level. The overall residual model-data misfits are close to the a priori errors (0.5°C and 5 cm , respectively). The ability to reproduce observed variability of pseudo wind stress anomalies is improved in the equatorial band as a result of the assimilation. However, the skill off the equator is rather limited. The residual model-data misfit in pseudo wind stress anomalies is larger than the a priori error of $10\text{ m}^2\text{ s}^{-2}$.

The forecasts of the 1997–1998 El Niño initialized from the assimilation product are more realistic than those without data assimilation. Consistent improvement due to the optimal initialization is found at least in the central-eastern equatorial Pacific for SST and sea level anomalies and in the central equatorial Pacific for zonal pseudo wind stress anomaly. Averaged over lead times of 1–12 months, the reduction of rms deviation from the data is $0.5^{\circ}\text{--}1^{\circ}\text{C}$, $4\text{--}7\text{ cm}$, and $5\text{--}10\text{ m}^2\text{ s}^{-1}$ for the three variables in the areas mentioned above. In terms of correlation with the data the level of improvement is 0.2 over most parts of the equatorial Pacific for SST and sea level anomalies and in the central equatorial Pacific for zonal pseudo wind stress.

The estimation of parameters plays a significant role in improving the model fit to the data both during the assimilation and the forecast. This is because the estimated drag coefficient and damping constants, determined inversely from data during the assimilation period, properly regulate the relative strength of forcing and damping of the anomalous ocean state. This enables the rapid development of a large amplitude warming event during the forecasts. Parameters values reported in the present study are estimated from a short period of data with an unprecedented magnitude of the anomalous state. Therefore they should not be considered as climatological values for the prediction of overall variability in previous data.

This initial attempt demonstrates the utility of several types of oceanic and atmospheric data for estimating the initial state and model parameters simultaneously in a coupled model context. The methodology is potentially useful to the initialization of ENSO forecast models as it minimizes initial shocks. It also highlights some limitations of such a simple coupled model in accounting for the observations and in delivering ENSO prediction even when several types of data are used in the initialization phase. There are several aspects that the optimal initialization did not (and will not) improve. These include the failure to predict the warming event before the westerly wind burst in March 1997 and the abrupt return to normal condition shortly after the easterly wind burst in May 1998, both of which present a grand challenge to the current ENSO forecast models. Improvement of the forward model is an indispensable step to bring about significant progress. For example, a better atmospheric component to reduce the large residual of model-data misfit in wind and to properly handle the asymmetry between warm and cold events.

Refinements of the assimilation scheme would also improve the estimates of model state and parameters and thus the forecasts. These include (1) a better prescription of the weighting for the model-data misfits to reflect model representation error and (2) explicit constraints of initial conditions and model parameters using appropriate weightings that accurately describe the uncertainties associated with the initial state and parameters.

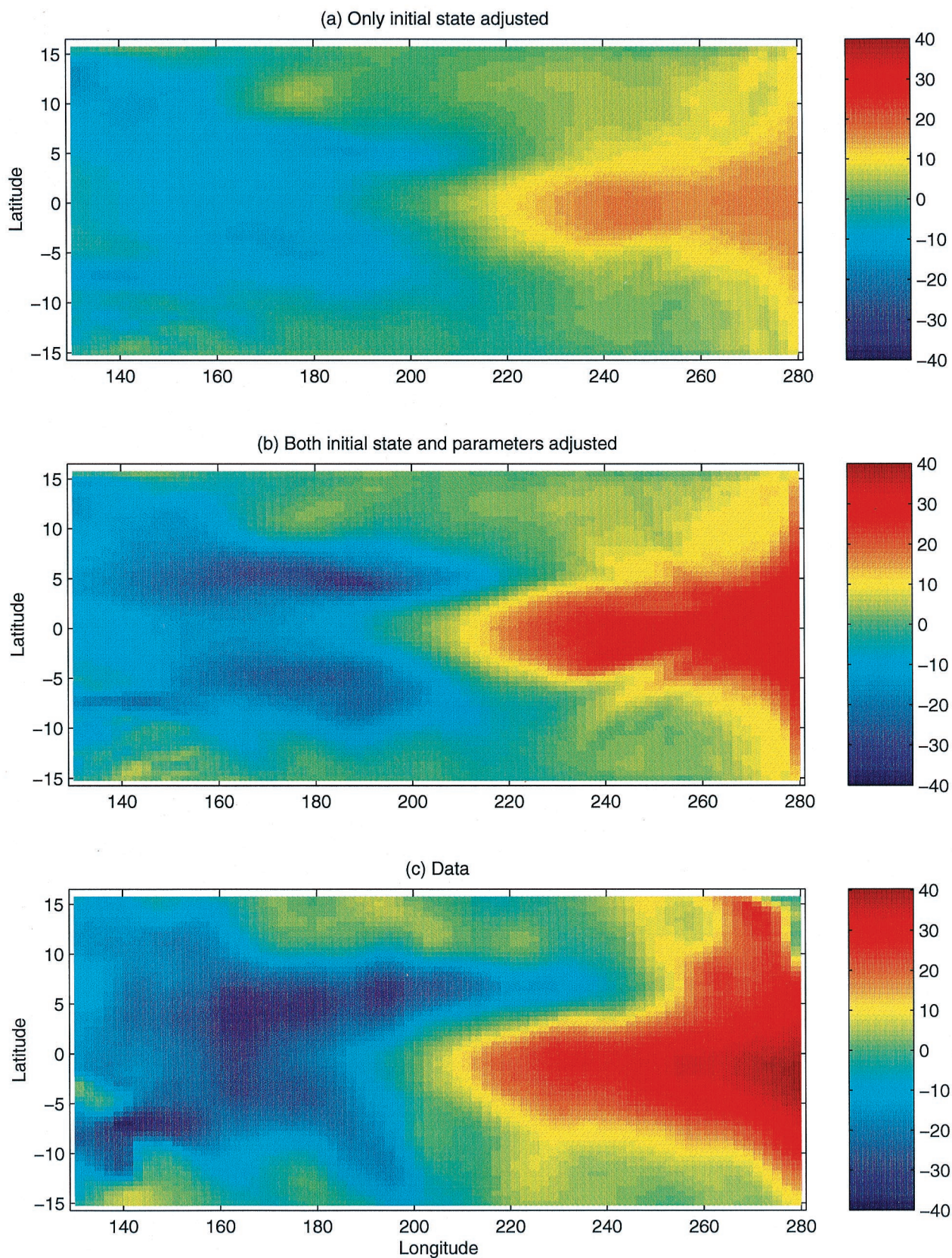


Plate 11. Estimated sea level anomalies in December 1997 derived from assimilation experiment from July 1997 to January 1998: (a) with only initial state adjusted, (b) with both initial state and parameters adjusted, and (c) the corresponding data.

Acknowledgments. This work was performed at the Jet Propulsion Laboratory, California Institute of Technology, supported by NASA under the Ocean Data Assimilation RTOP and TOPEX/Poseidon Project. The supercomputer used in this investigation was provided by funding from the NASA's Office of Earth Science, Aeronautics, and Space Science. We are thankful to C. Perigaud for her valuable comments during the course of the study.

References

- Barnett, T. P., M. Latif, N. Graham, M. Flugel, S. Pazan, and M. White, ENSO and ENSO-related predictability, I, Prediction of equatorial Pacific sea surface temperature with a hybrid coupled ocean-atmosphere model, *J. Clim.*, **8**, 1545–1566, 1993.
- Battisti, D. S., Dynamics and thermodynamics of a warming event in a coupled tropical atmosphere-ocean model, *J. Atmos. Sci.*, **45**, 2889–2819, 1988.
- Bennett, A. F., B. S. Chua, D. E. Harrison, and M. J. McPhaden, Generalized inversion of Tropical Atmosphere-Ocean (TAO) data and a coupled model of the tropical Pacific, *J. Clim.*, **11**, 1768–1792, 1998.
- Blumenthal, M. B., and M. A. Cane, Accounting for parameter uncertainties in model verification: An illustration with tropical sea surface temperature, *J. Phys. Oceanogr.*, **19**, 815–830, 1989.
- Boulanger, J.-F., The TRIDENT Pacific model, part I, The oceanic dynamical model and observations during the TOPEX/Poseidon period, *Clim. Dyn.*, in press, 2000.
- Cane, M. A., and R. J. Patton, A numerical model for low-frequency equatorial dynamics, *J. Phys. Oceanogr.*, **14**, 1853–1864, 1984.
- Cane, M. A., A. Kaplan, R. N. Miller, B. Tang, E. C. Hackert, and A. J. Busalacchi, Mapping tropical Pacific sea level: Data assimilation via a reduced state space Kalman filter, *J. Geophys. Res.*, **101**, 22,599–22,617, 1996.
- Chen, D., S. E. Zebiak, A. J. Busalacchi, and M. A. Cane, An improved procedure for El Niño forecasting, *Science*, **269**, 1699–1702, 1995.
- Chen, D., M. A. Cane, S. E. Zebiak, A. Kaplan, The impact of sea level data assimilation on the Lamont model prediction of the 1997/98 El Niño, *Geophys. Res. Lett.*, **25**, 2837–2840, 1998.
- Fu, L.-L., E. J. Christensen, C. A. Yamarone Jr., M. Lefebvre, Y. Menard, M. Dorrer, and P. Escudier, TOPEX/Poseidon mission overview, *J. Geophys. Res.*, **99**, 24,369–24,381, 1994.
- Giering, R., and T. Kaminski, Recipes for adjoint code construction, *Trans. Math. Software*, **24**, 457–474, 1998.
- Ji, M., and A. Leetmaa, Impact of data assimilation on ocean initialization and El Niño prediction, *Mon. Weather Rev.*, **125**, 742–753, 1997.
- Ji, M., A. Leetmaa, and J. Derber, An ocean analysis system for seasonal to interannual climate studies, *Mon. Weather Rev.*, **123**, 460–481, 1994a.
- Ji, M., A. Kumar, and A. Leetmaa, An experimental coupled forecast system at the National Meteorological Center: Some early results, *Tellus Ser. A*, **46**, 398–418, 1994b.
- Kirtman, B. P., J. Shukla, B. Huang, Z. Zhu, and E. K. Schneider, Multiseasonal predictions with a coupled tropical ocean-global atmosphere system, *Mon. Weather Rev.*, **125**, 789–808, 1997.
- Kleeman, R., On the dependence of hindcast skill in a coupled ocean-atmosphere model on ocean thermodynamics, *J. Clim.*, **6**, 2012–2033, 1993.
- Kleeman, R., A. M. Moore, and N. R. Smith, Assimilation of subsurface thermal data into a simple ocean model for the initialization of an intermediate tropical coupled ocean-atmosphere forecast model, *Mon. Weather Rev.*, **123**, 3103–3113, 1995.
- Large, W. G., and S. Pond, Open ocean momentum flux measurements in moderate to strong winds, *J. Phys. Oceanogr.*, **11**, 324–336, 1981.
- Levitus, S., Climatological atlas of the world ocean, *NOAA Prof. Pap.* **13**, 173 pp., U. S. Govt. Print. Off., Washington, D. C., 1982.
- Lorenc, A. C., Analysis methods for numerical weather prediction, *Q. J. R. Meteorol. Soc.*, **112**, 1177–1194, 1986.
- Neelin, J. D., A hybrid coupled general circulation model for El Niño studies, *J. Atmos. Sci.*, **47**, 674–693, 1990.
- Perigaud, C., and B. DeWitte, El Niño-La Niña events simulated with Cane and Zebiak's model and observed with satellite and in situ data, Part I, Model data comparison, *J. Clim.*, **9**, 66–84, 1996.
- Picaut, J., C. Menkes, J.-P. Boulanger, and Y. duPenhoat, Dissipation in a Pacific equatorial long wave model, *TOGA Notes* **10**, pp. 11–15, Nova Univ. Press, Dania, Fla., 1993.
- Reverdin, G., C. Frankignoul, and E. Kestenare, Seasonal variability in the surface currents of the equatorial Pacific, *J. Geophys. Res.*, **99**, 20,323–20,344, 1994.
- Smestad, O. M., and J. J. O'Brien, Variational data assimilation and parameter estimation in an equatorial Pacific Ocean model, *Prog. Oceanogr.*, **26**, 179–241, 1991.
- Smith, N. R., An improved system for tropical ocean subsurface temperature analysis, *J. Atmos. Oceanic Technol.*, **12**, 850–870, 1995.
- Syu, H.-H., J. D. Neelin, and D. Gutzler, Seasonal and interannual variability in a hybrid coupled GCM, *J. Clim.*, **8**, 2121–2143, 1995.
- Thacker, W. C., and R. B. Long, Fitting dynamics to data, *J. Geophys. Res.*, **93**, 1227–1240, 1988.
- Trenberth, K. E., W. G. Large, and J. G. Olson, The effective drag coefficient for evaluating wind stress over the oceans, *J. Clim.*, **2**, 1507–1516, 1989.
- Yu, L., and J. J. O'Brien, Variational estimation of the wind stress drag coefficient and the oceanic eddy viscosity profile, *J. Phys. Oceanogr.*, **21**, 709–719, 1991.
- Zebiak, S. E., and M. A. Cane, A model El Niño-Southern Oscillation, *Mon. Weather Rev.*, **115**, 2262–2278, 1987.

J.-P. Boulanger, Laboratoire d'Océanographie Dynamique et de Climatologie, CNRS, Université Paris VI, 75252 Paris cedex 05, France.

A. Foo, L.-L. Fu, R. Giering, and T. Lee, Jet Propulsion Laboratory, California Institute of Technology, 4800 Oak Grove Drive, Pasadena, CA 91109. (tleee@pacific.pl.nasa.gov)

(Received March 15, 1999; revised June 22, 2000; accepted June 27, 2000.)

